AD

EMBEDDED LDV MEASUREMENTS IN THE BOUNDARY LAYER OF MOVING WALLS

Final Technical Report

by

Christian. Maresca, Eric. Berton and Daniel. Favier

Laboratoire d'Aérodynamique et de Biomécanique du Mouvement
163 Av. de Luminy, Case 918
13288 marseille cedex 09. France

(December 2000)

United States Army

EUROPEAN RESEARCH OFFICE OF THE U.S. ARMY

London, England

CONTRACT NUMBER N 68171-99-M-6670

Contractor: M. Laurent, Président de l'Université de la Méditerranée

Approved for Public Release; distribution unlimited

20010502 083

REPORT DOCUMENTATION PAGE			
1.Agency Use Only	2.Report Date : 16 December 2000	3.Type of Report and Dates Covered : Final Report 16 Sept 99-15 Sept 00	
4.Titles and Subtitle: Embedded LDV measurements in the boundary layer of moving walls.			5.Funding Numbers : C N68171-99-M-6670 R-D8744-AN-01S
6.Author(s): C. Maresca, E. Berton, and D. Favier.			
7.Performing Organization Name(s) and Adresse(s) : LABM, CNRS-University of la Méditerranée. 163 Av. de Luminy, Case 918 13288 Marseille, Cedex 009, France			8. Performing Organization Report Number : 99-12-16-8
9.Sponsoring/Monitoring Agency Name(s) and Adresse(s)			10. Sponsoring/Monitoring Agency Report
11.Supplementary notes			
12a.Distribution/Availability Statement : public availability			12b.Distribution Code

13.Abstracts : Smoke visualization and embedded laser velocimeter operating in the backscatter mode were used to survey the flow about wings oscillating through stall in the Luminy wind tunnels S1L and S2L.

The experiments were carried out about rectangular wings with an NACA 0012 airfoil section at nominal Reynolds numbers $R_e=10^5$, 210^5, and 10^6. During the oscillation, the wing angle of attack was varied around mean values α_0 deg= 6; 15; and 21; through an amplitude $\Delta\alpha=\pm$ 6deg, and a reduced frequency k=0.188.

Pictures and movies realized using the laser sheet technique have shown that the features of dynamic stall are independent of Reynolds numbers, at least in the present experiments ($10^5 \leq R_e \leq 10^6$). Effects of upstroke and downstroke on separation and reattachment of boundary layer are clearly shown as well as deviation from steady behavior analyzed at the same angle of attack for fixed and oscillating airfoil.

The measurements of two orthogonal components of instantaneous velocity through the boundary layer along a normal to the surface of the wing have shown that the embedded laser velocimeter is well suited to characterize qualitatively and quantitatively the structure of the boundary layer (laminar, transition, turbulent) as well as strong separation with leading edge bubble involved during dynamic. These results constitute a useful data base for future computational unsteady boundary layer.

14.Subject terms: Dynamic stall. Boundary layer. Visualization. Laser light sheet. Image processing.	15.Number of Pages
	16.Price Code

17.Security Classification Unclassified	18. Security Classification of this Page Unclassified	19.Security Classification of Abstract Unclassified	20.Limitation of Abstract UL

SUMMARY

Smoke visualization and embedded laser velocimeter operating in the backscatter mode were used to survey the flow about wings oscillating through stall in the Luminy wind tunnels S1L and S2L.

The experiments were carried out about rectangular wings with an NACA 0012 airfoil section at nominal Reynolds numbers $R_e=10^5$, 210^5, and 10^6. During the oscillation, the wing angle of attack varied around mean values α_0=6deg and 15deg through an angle amplitude $\Delta\alpha=\pm$ 6deg, at reduced frequency k=0.188.

Pictures and movies realized using the laser sheet technique have shown that the features of dynamic stall are independent of Reynolds numbers, at least in the present experiments ($10^5 \leq R_e \leq 10^6$). Effects of upstroke and downstroke on separation and reattachment of boundary layer are clearly shown as well as deviation from steady behavior analyzed at the same angle of attack for fixed and oscillating airfoil.

The measurements of two orthogonal components of instantaneous velocity through the boundary layer along a normal to the surface of the wing have shown that the embedded laser velocimeter is well suited to characterize qualitatively and quantitatively the structure of the boundary layer (laminar, transition, turbulent), as well as strong separation with leading edge bubble involved during dynamic stall. These results constitute a useful data base for future computational unsteady boundary layer.

List of Keywords: Dynamic stall, Boundary layer, Bubble separation, Laser light sheet visualization, Embedded Laser Doppler Velocimeter, Image processing.

INTRODUCTION

The loading of an airfoil during dynamic stall has been extensively investigated. The features of the stalling process, typical of the retreating blade of a helicopter rotor in forward flight, have been delineated several years ago on airfoils oscillating either in pitch[1-3] or in fore and aft-pitching combined motion[4-6]. More recently, W. G. Bouseman[7] has shown that the loading, characterized by the peak airfoil lift and drag, and the minimum pitching moment, termed the "dynamic stall function", is similar over a wide range of test conditions including flight tests. In particular, the dynamic stall function appears to be relatively insensitive to Reynolds number and shows that an accurate prediction of 3-D effects is not of prime importance for the prediction of dynamic stall on a flight vehicle.

These results encourage to enforce numerical methods presently developed for the direct calculation of dynamic stall by solving the Navier-Stokes equation[9] but limited to 2D flow at low Reynolds Number. These challenging methods are at a research stage and their validation and improvement require more accurate and suited experimental data. Particularly, phenomena occurring in the region very close to the blades, like bubble formation, transition and separation, require local and detailed information from the boundary layer (BL). Among these informations, visualization and instantaneous velocity profiles remain one of the main useful and suitable tools for analyzing the behavior and the structure of BL.

The present experimental study, done at LABM (Laboratoire d'Aérodynamique et de Biomécanique du Mouvement) from the University de la Méditerranée, proposes to contribute to the numerical and theoretical developments undertaken in this research field at the Aeromechanics of the Army/NASA Rotorcraft Division. The experimental results provided on BL velocity profiles and on the structure of unsteady separated flows have been mainly based on measurements using a unique embedded LDV technique. LABM has developed for 5 years original types of embedded LDV for measurements of oscillating profile and rotary wings boundary layer[6],[9]. Concerning oscillating profiles[6] (NACA0012, 0.3m in chord), the velocity components have been measured in 2D and 3D configurations by help of a LDV embedded in the oscillating frame, in such a way that the velocities are directly measured in a reference frame in relative motion. Concerning hovering helicopter rotor blades[9], BL measurements have been performed in a frame linked to the rotating blade for one radial distance from the rotation axis and at a chord abscissa x/c=0.25.

The aim of the present seed proposal (first phase) was to show that the embedded LDV applied to a blade profile oscillating through dynamic stall is well suited to study qualitatively and quantitatively the physics of unsteady separated flows.

This preliminary study has been undertaken in 2 different wind tunnels (S1L and S2L of LABM) at 3 Reynolds numbers (10^5, 2.10^5 and 10^6) corresponding to 3 Mach numbers (0.015, 0.030 and 0.15). The airfoil was oscillating in pitch through dynamic stall around a mean angle of attack α_0, at a reduced frequency k and an amplitude of incidence $\Delta\alpha$ relevant to the retreating helicopter rotor blade (k=0.188, α_0=6deg and 15 deg, $\Delta\alpha$=6deg).

A particular attention has been paid in this first phase to the structure of the flow field when the angle of attack is increasing and decreasing through the separated and reattached BL regimes.

The formation and shedding of vortices generated by the dynamic stall have been observed using a laser sheet visualization technique. Movies showing separation and reattachment during dynamic stall have been compared at $Re=10^5$ 2.10^5 and 10^6.

The two velocity components ($U=U(\omega t)$, and $V=V(\omega t)$) have been measured in the BL from y=0.3mm at the wall to 100 mm outside of the BL. Inside the BL, measurements have been performed at every altitude step of 0.2 mm.

SYMBOLS

C	Airfoil chord, m
f	frequency, Hz
h	Airfoil span, m
k	reduced frequency, $k=C\omega/2U_\infty$
Re	Reynolds number, $Re=U_\infty C/\nu$
U_∞	Wind tunnel velocity, m/sec
U,V	Tangential and normal velocity, m/sec
s	Curvilinear abscissa, m
t	Time, sec
x, y	Tangential and normal coordinate at the airfoil surface, m
α	Angle of attack of the airfoil, deg
α_0	Mean angle of attack, deg
$\Delta\alpha$	Amplitude of the pitching oscillation, deg
δ	Thickness boundary layer, m
η	Reduced normal coordinate, $\eta=y(Re_x)^{1/2}/x$
ω	Rotational frequency, rad/sec

EXPERIMENTAL INVESTIGATION

The wind tunnels

-S1Luminy high speed (Fig.1) is a closed circuit wind-tunnel with octagonal closed test-section (inside circle of 3m), 6m in length, free stream velocity varying from 5m/s to 100m/s; constant temperature of the flow within the test section : $\Delta t<1°C$; natural turbulence intensity lower than 0.3% (longitudinal) and 0.1% (transversal).

-S2Luminy low speed (Fig.2) is an open circuit wind-tunnel with rectangular closed section (1mx0.5m) 3m in length, free stream velocity varying from 2.5m/s to 25m/s, natural turbulence intensity less than 0.5%.

Oscillating airfoils

Airfoils used in both wind tunnels are of NACA0012 profile. One of them, experimented in S1L, is 0.488m in chord, 1 m in height, with one tip mounted flush to the floor of the test section, the other tip is equipped with an end plate in order to simulate a like 2-D flow at mid span. The pitching motion of the airfoil is allowed by means of an oscillating device located under the test section (see Fig.1) and supporting vertically the model by means of a support shaft located at the quarter chord axis. In this way, the instantaneous incidence $\alpha(t)$ of the airfoil is given by:

$$\alpha(t)= \alpha_0+\Delta\alpha\sin(\omega t),$$

where α_0 is the mean incidence and ω the rotational frequency.

The airfoil used in S2L (0.30m in chord and 0.50m in height) is mounted vertically and spans the entire test section. This airfoil is supported at the quarter chord axis by an oscillating device (see Fig.2) which allows a combined motion of fore and aft and pitching motion. In the present case only the pitching motion was used, giving the same variation of the instantaneous incidence as in S1L.

The following table summarizes the experimental conditions realized in S1L and S2L:

Table 1

	U_∞: m/s	Chord C: m	Re	$f=2\pi/\omega$: Hz	k	α_0: deg	$\Delta\alpha$: deg
S1L	31	0.48	10^6	3.8	0.188	21	6
S2L	5	0.3	10^5, 210^5	1	0.188	6, 15	6

Visualization

The technique consists in illuminating the mid-span of the airfoil while the flow is seeded upstream with oil smoke emitted through a tube rake. The light sheet is produced from an optical system mounted flush

with the wall of the wind tunnel in order to avoid light reflection. The optical system, manufactured by Dantec, is composed of a glass cylinder and a converging lens connected by an optical fiber to a laser source (Spectra-Physics 12 Watts). Figure 3 shows, as an example, the set-up realized in S2L. It can be seen that the light sheet has been adjusted to illuminate the middle horizontal plane of the wind tunnel. During tests, pictures of the flowfield close to the airfoil are taken from a digital camera (Olympus Camedia C-2500L) synchronized on the motion of the oscillating airfoil. These pictures are processed through "Adobe Photoshop" software in order to capture the features of the flowfield. Moreover, movies have been realized from the pictures shot at different instant of the period of oscillation.

The same technique described above has been used in S1L.

Velocity measurements

For each chordwise section selected, the flow survey is performed along the local normal to the wall surface (the altitude Y ranging from about 0.3 mm to 100mm).

The Embedded Laser Doppler Velocimeter[6] (ELDV) used for this survey has an optical head mounted on a supporting turntable linked to the oscillating frame as sketched in Fig.1 and 2. Moreover, it is equipped with a beam-expander to increase the focal distance to 400mm. This optical head is installed on an automated 2D-displacement device mounted itself on the turntable. The laser beams are so focusing from a 45deg mirror in the boundary layer at the span wise locations considered. The supporting turntable is linked with the oscillating frame, so that U and V velocity components can be directly measured in the same reference frame than the oscillating BL. A teledriven system allows the adequate positionning of the measurement volume at any point of the airfoil surface (30cm in chordwise displacement). An angular sector provides the selection of the surveying normal direction, and the laser measurement volume can be displaced along the local normal to the surface from y = 0.3mm to y = 145mm with a displacement accuracy of 0.1mm.

Due to the periodicity of the flow, each period is considered as a specific sample of the same phenomenon. So, each velocity component is recorded at each phase angle ωt comprised between 0deg and 360deg by step of 1deg over a large number of periods. Data are then statistically analyzed at prescribed values of the period, e.g. the instantaneous incidence, with a precision of $\delta\alpha=4\Delta\alpha/360=24/360=0.066$deg. The acquisition time is stopped when 19,564 data have been stored, that generally requires about 150 periods.

Data acquisitions are made on a microcomputer from two Burst Spectrum Analyser delivering the values of the two components U and V and the arrival validation time for each frequency measurement. The software used for acquisition and data reduction (COMBSA) has been developed at LABM under Apple LabVIEW system.

RESULTS AND DISCUSSION

Visualizations

The visualizations have been performed owing to the technique described above. The experiments have been duplicated in S1L and S2L, in order to investigate Reynolds numbers ranging from 10^5 to 10^6.

Both steady and unsteady case have been studied. In the steady case, pictures of the flow on the upper side of the profile were taken from the digital camera (Olympus Camedia C-2500L) for values of the incidence varying from 0deg to 21deg by step of 1deg. Two Reynolds numbers were explored ($R_e = 10^5$ and 2.10^5) in S2L and one ($R_e = 10^6$) in S1L. Movies representing one cycle of "quasi-steady" oscillation, has been realized from the successive steady pictures corresponding to α_0 increasing from α= 9deg to 21deg and back to 9deg by step of 1deg in S2L and from 15deg to 27deg and back in S1L.

In the unsteady case, pictures of the upper side flow field were shot at different instant of the period when the airfoil oscillated in pitch through dynamic stall at parameters of table 1, and movies of successive pictures have also been realized.

Low Reynolds numbers

As examples, Figures 4 to 7 shows steady and unsteady results at two angles of attack. One of them (α_0=10deg) corresponds to unstalled regime, the other (α_0=14deg) to stall regime. In each figure, the upper picture corresponds to the steady case, the middle one to the pitching airfoil at the same incidence in downstroke, the lower to the airfoil in upstroke. Figures 4-5 are relative to $R_e=10^5$ and Fig 6-7 to $R_e=210^5$. Useful comparisons can be made from these figures: for the range of variation presented here, it can be said that the effect of Reynolds number on the phenomenon seems not to be significant. Reattachment of boundary layer during downstroke occurs from leading edge to trailing edge and is very close to steady flow (Figs 4 to 7), though during upstroke, for the 2 Reynolds numbers studied (Fig.4 and 6), separation seems to occur at 10deg with the formation of a high vorticity flow, sustaining as it is well known a high level of lift until the maximum incidence is reached.

Two movies showing the successive phases of the period of oscillation have been realized: one when the airfoil oscillates in a like "quasi-steady" flow, the other when the airfoil undergoes the unsteady dynamic

stall. The deviation from steady behavior due to unsteadiness effect involved by dynamic stall is underlined by comparison between the two movies.

High Reynolds number

Experiments performed in S1L have concerned a rectangular wing of the same NACA 0012 airfoile used in S2L.The wing of 0.86m in height, and 0.48m in chord spans only part of the test section. It seemed interesting to test such a model at $Re=10^6$ in order to evaluate both the effects of Reynolds Number and 3-dimensionnality induced by the wing tip by comparing the results to those obtained in S2L in 2D configuration at lower Reynolds Numbers. In these new experimental conditions, static stall incidence of the wing is about 21deg, compared to 12deg in 2D case. The parametric conditions of pitching around a mean incidence α_0 =21deg are: $\Delta\alpha=\pm 6$ and k=0.188.

Figures 8 to11 show some of the visualization pictures realized at incidences varying between 15deg and 27deg. In Figures 8 and 9, the effects of dynamic stall occurring at 18deg and 21deg during downstroke and upstroke are presented and compared to the static values. It can be clearly seen that during downstroke the reattachment of the boundary layer concerns a large part of the upperside from leading edge to trailing edge. During upstroke, a separation of the flow consecutive to the reattachment process is characterized by a high vorticity level generated by a large bubble at leading edge (α=21deg).

In Figure 10, the flow is reattached at lower incidence (α=16deg) with the same feature than in steady configuration. Nevertheless, when the maximum incidence is reached at 27deg (Fig. 11), the stall experimented by the airfoil in unsteady case is deeper than the one occurring at static incidence and exhibits the high vorticity flow previously mentionned.

Visualizations realized at different Reynolds Numbers ranging from 10^5 to 10^6 on 2D and 3D wings oscillating at the same reduced frequency reveal the same features of the dynamic stall: reattachment during downstroke from leading edge to trailing edge, and separation of the flow with strong vorticity during the end of the upstroke generated by a leadiung edge bubble.

It can be concluded than variation of Reynolds effects in a range 10^5-10^6 and tip wing do not seem to affect the structure of dynamic stall at least at k=0.188. This remark is in good agreement with some conclusion given in the paper by W. Bouseman[7].

Visualizations have shown that separated flows occurring on the upper side of the airfoil oscillation at high angle of attack result from the bursting of a leading edge bubble. On the other hand, when the airfoil oscillates through lower incidences with no separated flow ($\alpha\leq$12deg), a bubble remains located close to the leading edge, but its size is too small to be well defined by the image processing. However, it will be shown here after that the analysis of velocity profiles recorded through the boundary layer can result in the quantitative definition of the laminar separation bubble. The analysis is based on the fact that when the flow is seeded upstream, only very few particles can enter into the bubble. Thus, when the measuring volume is inside the bubble, the rate of data acquisition over several periods remains close to zero resulting in a no data zone observed on the velocity records. This no data zone allows determining the height of the bubble and the incidence at which the bubble enters into the measuring volume location.

Velocity profiles at low incidence ($0\leq\alpha\leq$12deg) and low Reynolds number ($Re=10^5$)

As explained before, the lack of data on time-velocity records reveals the presence of a bubble. Velocity components $U=U(\omega t)$ and $V=V(\omega t)$, have been recorded for different location Y of the measuring volume (Ymm=100; 80; 60; 40; 30; 20; 10; 8; 6; 4; 2; 1; 0.8; 0.6; 0.4), at different chord location x/C=0.1; 0.2; 0.3; and 0.67.

Figure 12 gives an example of cumulative (more than 300 periods) velocity records with incidence at x/C=0.1 obtained at different distance from the wall. It can be seen no lack of data far from the wall (Y=10mm) when the incidence varies from 12deg to 0 and back to 12. When approaching the wall (from Y=3mm to Y=0.6mm), a zone of "no data" indicative of a separation bubble can be observed during downstroke and upstroke. It has thus been possible to determine the height of the bubble at a given incidence for different chord locations from 0.1 to 0.67.

Figure 13 shows the variation with the airfoil incidence of the size of the separation bubble during downstroke and upstroke deduced from the different velocity records. It can be observed that for $0\text{deg}\leq\alpha\leq$12deg, the separation bubble remains located near the leading edge ($0\leq x/C\leq 0.3$), as no bubble has been identified at x/C=0.3 and 0.67 (see Fig.13). The maximum size of the bubble can be evaluated and is shown to vary between 6mm (Y/C=0.02) in downstroke and 3mm (Y/C=0.01) in upstroke.

Velocity profiles $U(Y,\alpha)$, $V(Y,\alpha)$, have been statistically analyzed from the time-velocity records at different instants of the period corresponding to different values of airfoil incidence α. Although useful information could have been carried out from the $V(Y,\alpha)$ component that constitutes with $U(Y,\alpha)$ a valuable data base to be analyzed in more detail later, only some typical results of the $U(Y,\alpha)$ component have been analyzed in the frame of this report. Figure 14 shows as an example the results obtained on $U(Y,\alpha)$ at x/C=0.1,

0.2, 0.3 and 0.67 for 6 values of α= 0 and 12deg on the top of the figure, 6 and 9deg during downstroke on the left, and during upstroke on the right. It can be seen that the boundary layer velocities obtained at x/C=0.67 are not influenced all along the period by a bubble eventually located at this chord station. A more accurate analysis of the results shows that these profiles are typical of a turbulent boundary layer ($U(Y)=kU^{(1/n)}$). On the other hand, velocity profiles close to the leading edge (x/C=0.1; 0.2; 0.3) are affected by the bubble particularly at x/C=0.1 when α=12 and 9deg during the downstroke and show a lack of values in the boundary layer (Y<2mm). At such incidences, the bubble induces transition of the BL that is characterized by scattered results inside the B.L. During upstroke the bubble effect weakens at x/C=0.1 as it can be seen at α=9deg, due to the weakness of the bubble in upstroke at shown in Fig. 13. Moreover the variations of the potential velocity (Y>10mm) with x/C and incidence are in good agreement with the variations of the known pressure distribution over the upper side of a NACAOO12 airfoil (suction pick close to x/C=0.1).

Although very few particles can enter into the bubble (see Fig.12), it has been possible, allowing to a long time consuming process, to record velocity profiles in the bubble. This test was made at x/C=0.2, α=9deg in downstroke, where the thickness of the bubble is 2mm (Fig.13). It is shown in Fig.15 that the velocity profile measured from the wall to the potential flow exhibits a reverse flow due to the vortex inside the bubble. On the same figure is also presented the velocity profile of a typical attached B.L., measured at x/C=0.3, where no reverse flow is observed.

Velocity profiles at high incidence (9deg$\leq\alpha\leq$21deg) and low Reynolds number ($Re=10^5$)

In the case where dynamic stall occurs during the oscillation (9deg$\leq\alpha\leq$21deg), the separation region is characterized by velocity records analogous to those presented as long as the bubble was concerned at low incidence. The analysis of data lack on velocity realized at x/C=0.2; 0.3; and 0.67 allows determining at a given incidence of the oscillation the mean value of the bubble dimension normal to the surface airfoil. The dimensions of the bubble deduced from velocity records are presented by white segments in Figure 16 at incidences α=12; 14; and 18deg. These results compared to visualizations show a good agreement although they concern averaged (velocity records) and instantaneous (visualizations) values. Bubbles as high as 100mm (Y/C=0.3) have been measured.

Results obtained on the $U(Y,\alpha)$ component at x/C=0.2; 0.3; and 0.67 are presented in Figure 17 for 6 values of α:

-9deg and 21deg on the top of the figure, corresponding to maximum and minimum values of the incidence during the oscillation,

-15deg and 18deg as typical examples of incidences during downstroke (on the left), and upstroke (on the right).

It is worthy to note that during downstroke at high incidence (15deg$\leq\alpha\leq$18deg) the separation can be pointed out by a no data recorded zone at leading edge resulting in no value of $U(Y,\alpha)$ on the plots relative to x/C=0.2, and 0.3. Nevertheless, a reverse flow due to vortices is shown at x/C=0.67, characterized by negative values of $U(Y,\alpha)$.

At minimum incidence (9deg), and during upstoke α=15deg, it has been possible to perform velocity measurements very close to the wall; results obtained are typical of a reattached flow with boundary layer. Profiles obtained at higher upstroke incidence (α=18deg), reveal a bubble located at leading edge and a flow reattachment at x/C=0.67, due to the vortex induced at leading edge during upstroke.

Velocity profiles at high incidence (15deg$\leq\alpha\leq$27deg) and high Reynolds number ($Re=10^6$)

Velocity records from laser velocimeter performed at $Re=10^6$ in S1L concern 2 chord stations: x/C=0.4 and 0.6. For each value of x/C, velocity measurements have been done at the following altitudes:Ymm=80; 60; 40; 20; 10; 8; 6; 4; 2; 1.5; 1; 0.8; and 0.6.

Analyzing the records as those presented in Fig 12 can carry out qualitative information. A region where the flow is reattached is characterized by a large number of no scattered data acquired during several periods of oscillation. The values measured at the different altitudes allow to plot the velocity profiles of U, and V, from outside to the airfoil surface. When the wing is undergoing dynamic stall with strong vorticity flow occurring on the upperside, records show that the regions explored are scattered over with less data. In this case, velocity profiles become less accurate. Figure 18 presents as an example data records obtained at X/C=0.4 (top of the figure), and X/C=0.6 (bottom), for Ymm=80. It can be seen that the region close to 21deg upstroke is scattered over with data, in accordance to Fig 11 where the flow shows a high vorticity at this incidence. At 21deg downstoke, the data are gathered around the mean value of the flow, attesting of a reattached flow as shown in the Fig.11. Same comments can be made at 18deg up and down, and 16deg down (Figs.8-10). Concerning 27deg, the flow at Y=80mm seems to be potential, as shown in Fig. 11 where Y=80mm is very close to the boundary of the undisturbed flow.

Figure 19 shows some examples of the U (Y,α) profiles deduced from data records as those presented in Fig18 and concern incidence where the scatter of data remains low enough between 27deg and 18deg in downstroke to allow an accurate measurement of the velocity. Fig.19 gives the velocity profiles obtained by averaging the velocity results at 27; 21 and 18deg. As the incidence decreases from 21deg to 18deg it becomes more difficult to obtain useful values close to the wall, as shown by the lack of data on the plots.

CONCLUSIONS

Two wings of NACA 0012 airfoil oscillating in pitch has been tested in 2D and 3D configurations at Reynolds Numbers ranging from 10^5 to 10^6. The mean angles of attack were α_0=6; 15 and 21deg, the angular amplitude $\Delta\alpha$=±6deg and the frequency oscillation k=0.188.

Smoke filaments emitted from upstream visualized the flow on the upper side of the airfoil, illuminated by a laser sheet. Pictures of the flowfield were taken at different instants of the oscillation by use of a numerical camera and movies were realized from the pictures.

Measurements of axial and radial components of the velocity were performed using an embedded laser velocimeter. The velocity survey was made normally to the airfoil surface, from 100mm outside to 0.4mm to the wall.

The different features of the flow around the oscillating airfoil has been analyzed both from visualizations and velocity measurements. It has thus been possible to quantitatively characterize a separation bubble close to the leading edge when the wing oscillates at low incidence (less than 12deg). The bubble remains located at the third front part of the upperside with a normal dimension to the wall Y/C varying between about 0.02 and 0.01 during respectively downstoke and upstroke.

At higher incidence, pictures and velocity measurements have shown the different features experienced by the flow during downstroke and upstroke as reattachment, large separation bubble, and high vorticity flow.

The comparisons made on the results obtained in different conditions seem to point out that the effects of Reynolds numbers in the range 10^5-10^6, and of the tip wing are very weak, as already remarked by W. Bouseman[7].

Although velocity results presented in the frame of the present report concern only the U component, a database made of both U (α, Y) and V (α, Y) has been constituted that will be very useful in computational unsteady boundary layer.

This study has clearly shown that embedded laser velocimetry is a suitable and useful tool to investigate unsteady boundary layer and dynamic stall regime occurring on oscillating airfoils. In the future, it is intended to emphasize on the measurement of the turbulence components.

REFERENCES

1. W. J. McCroskey, K. W. McAlister, L. W. Carr, and S. L. Pucci, "An Experimental Study of Dynamic Stall on advanced Airfoils sections Volume 1. Summary of Experiments",
NASA TM 84245, July 1982.

2. K. W. McAlister, S. L. Pucci, W. J. McCroskey, and, L. W. Carr, "An Experimental Study of Dynamic Stall on advanced Airfoils sections Volume 2.Pressure and Force Data"
NASA TM 84245, September 1982.

3. L. W. Carr, W. J. McCroskey, K. W. McAlister, S. L. Pucci, and O. Lambert, "An Experimental Study of Dynamic Stall on advanced Airfoils sections Volume 3.Hot wire and hot film measurements "
NASA TM 84245, December 1982.

4. C. Maresca, D. Favier, and J. Rebont, "Unsteady Aerodynamics of an Airfoil at High Angle of Attack Performing Various Linerar oscillations in Uniform Stream."
Journal of American Helicopter society, Vol.20, n°7, pp. 865-871, 1982

5. D. Favier, A. Agnes, C. Barbi, and C. Maresca, "The combined Translation-Pitch Motion of a New Airfoil Dynamic Stall Simulation",
Journal of Aircraft, Vol.25n° 9, pp. 805-814, 1988.

6. E. Berton, D.Favier, C.Maresca, "Embedded L.V. methodology for boundary-layer measurements on oscillating models", A.I.A.A., Proceedings of the 28th Fluid Dynamics Conf., A.I.A.A. paper n° 97/1832, Snowmass, June 1997.

7. W. G. Bouseman, « Evaluation of Airfoil Dynamic Stall Characteristics for Maneuverability", 26th European Rotorcraft Forum, The Hague, Netherland, September 26-29, 2000.

8. D.Favier, C.Maresca, M. Nsi Mba, E. Berton, A.Agnes, "New Type of Embedded Laser Doppler Velocimeter (ELDV) for Measurement of Rotary Wings Boundary-Layer", The Review of Scientific Instruments, Vol. 66, n° 6, pp. 2447-2455, 1997.

9. K. Pahlke, E. Chelli, "Calculation of Multibladed Rotors in Forward Flight Using 3D Navier-Stokes Method", Proceedings of the 26TH European Rotorcraft Forum, 26-29 September 2000, The Hague, The Netherlands.

Fig. 1

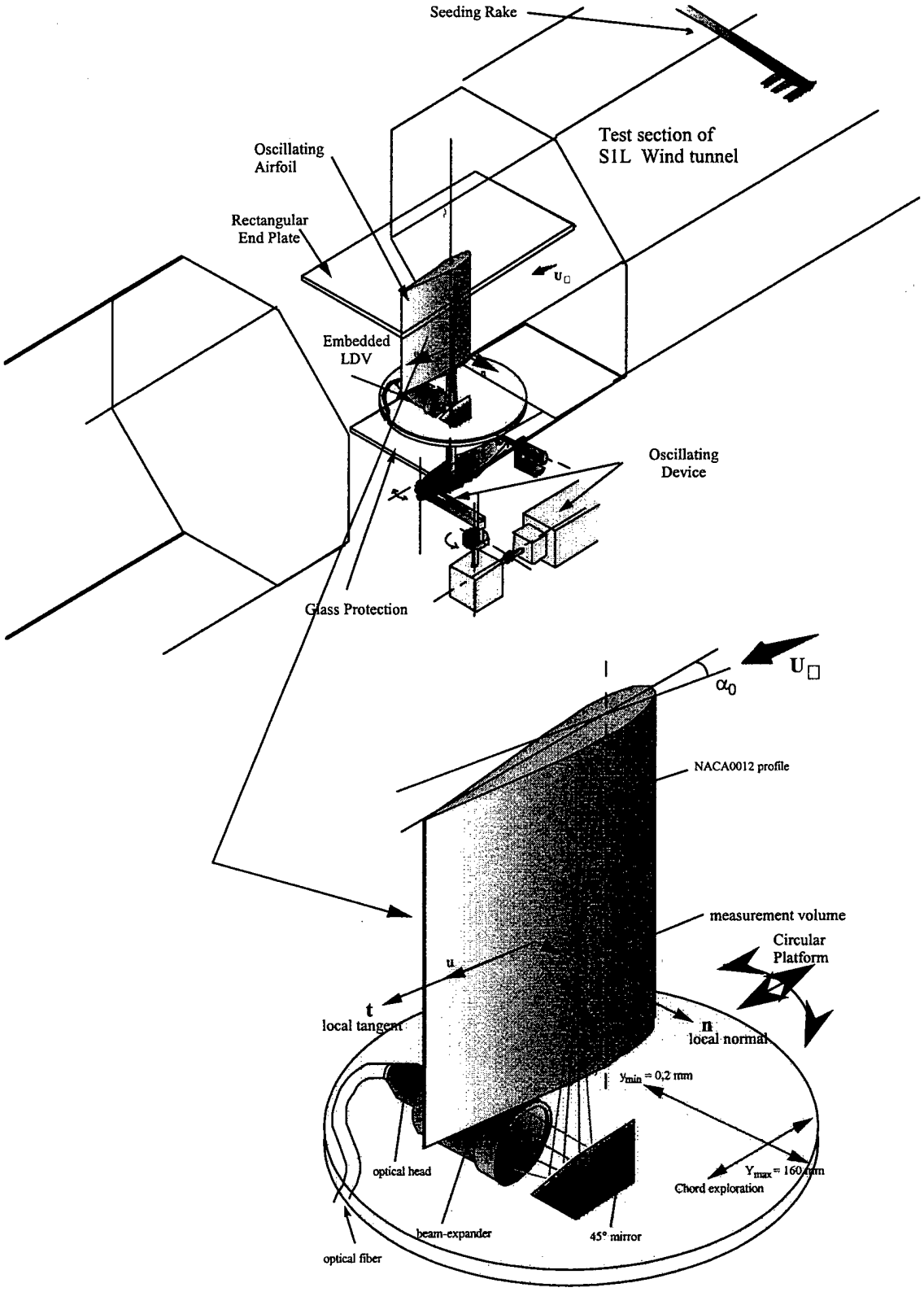
Seeding Rake
Test section of
S1L Wind tunnel
Oscillating
Airfoil
Rectangular
End Plate
U_∞
Embedded
LDV
Oscillating
Device
Glass Protection
U_∞
α_0
NACA0012 profile
measurement volume
Circular
Platform
u
t
local tangent
n
local normal
y_{min} = 0,2 mm
optical head
Y_{max} = 160 mm
Chord exploration
beam-expander
45° mirror
optical fiber

Fig. 2

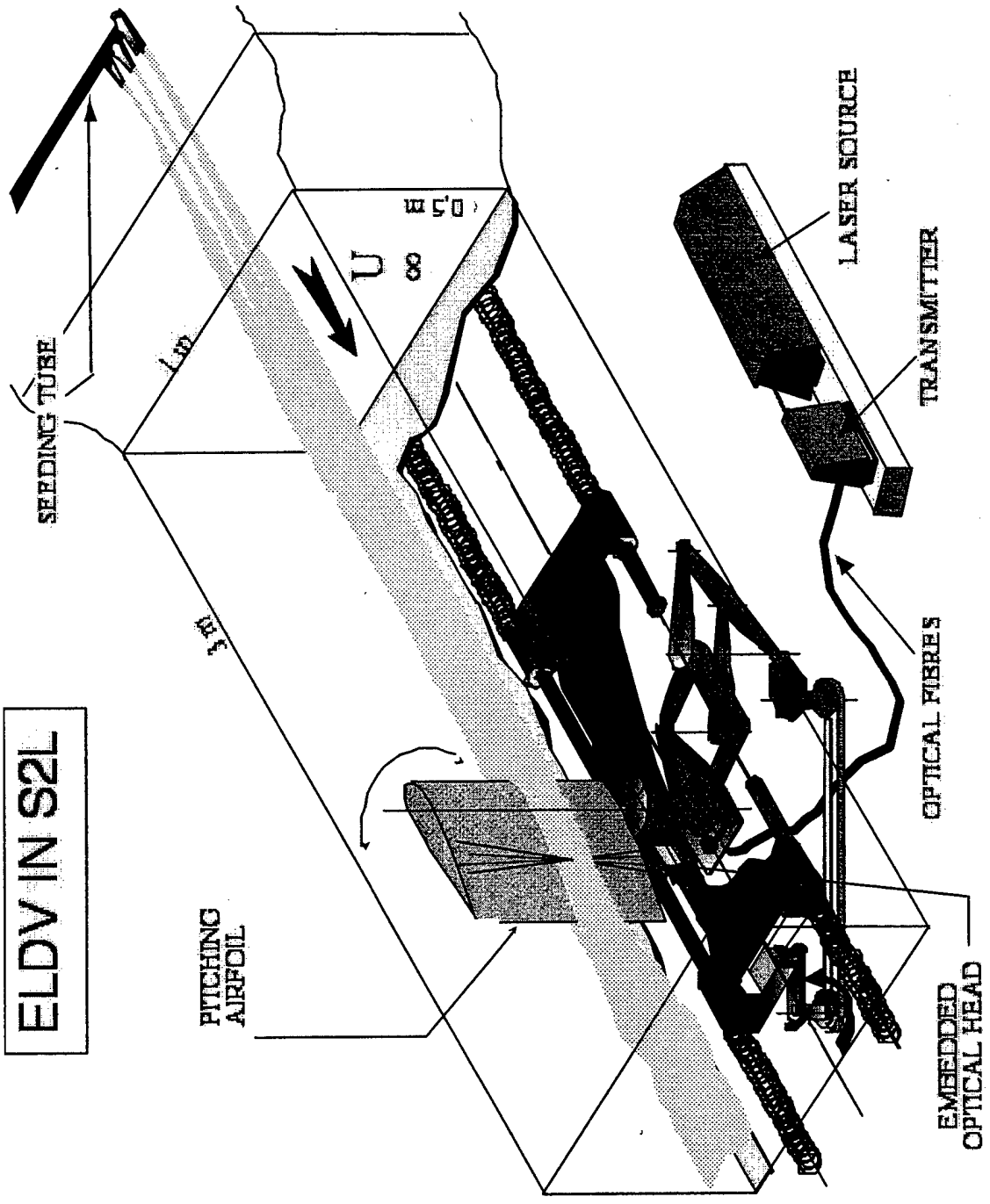
ELDV IN S2L
SEEDING TUBE
PITCHING AIRFOIL
LASER SOURCE
TRANSMITTER
OPTICAL FIBRES
EMBEDDED OPTICAL HEAD

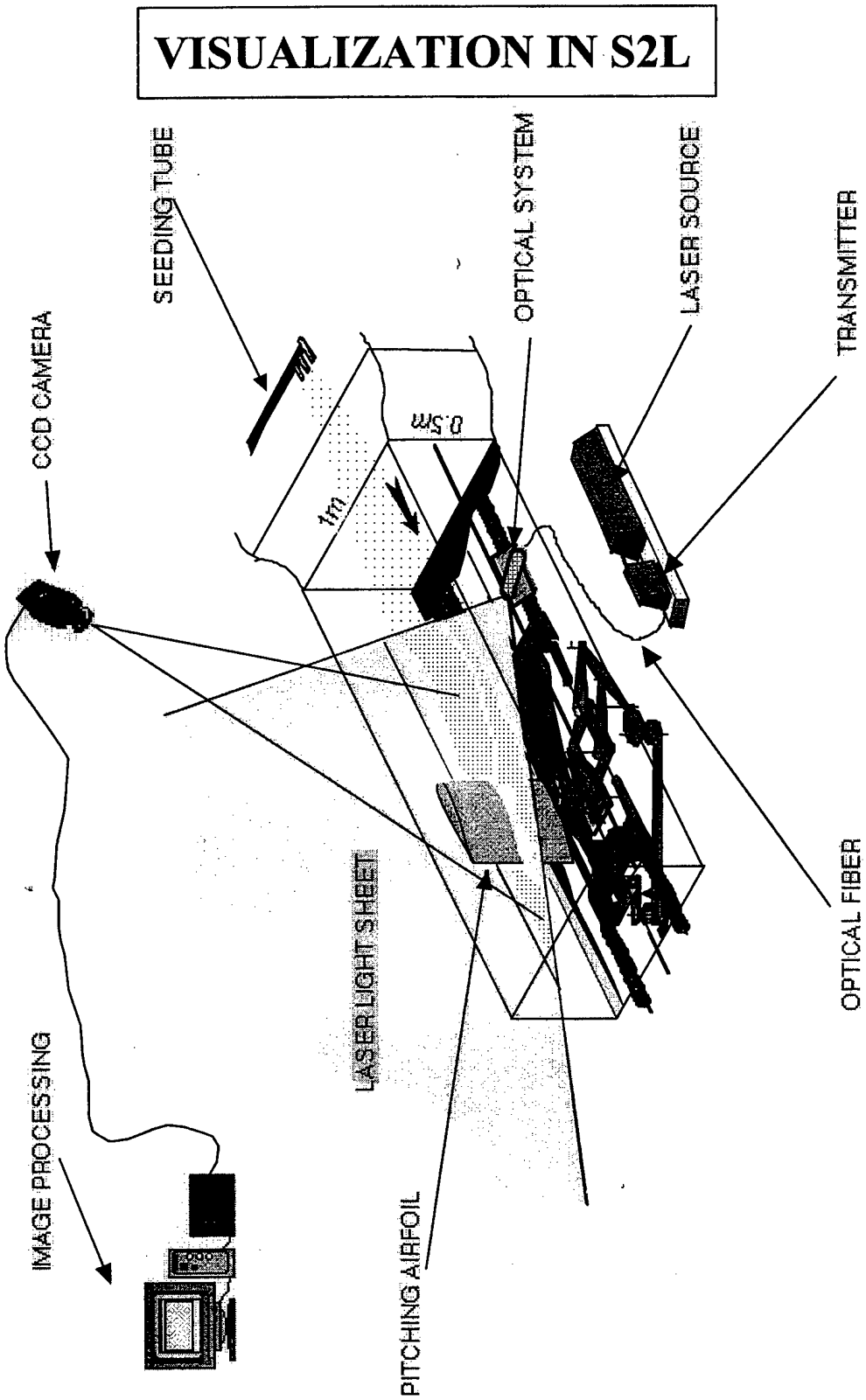
VISUALIZATION IN S2L
SEEDING TUBE
OPTICAL SYSTEM
LASER SOURCE
TRANSMITTER
CCD CAMERA
0.5m
1m
LASER LIGHT SHEET
OPTICAL FIBER
IMAGE PROCESSING
PITCHING AIRFOIL

Fig 3

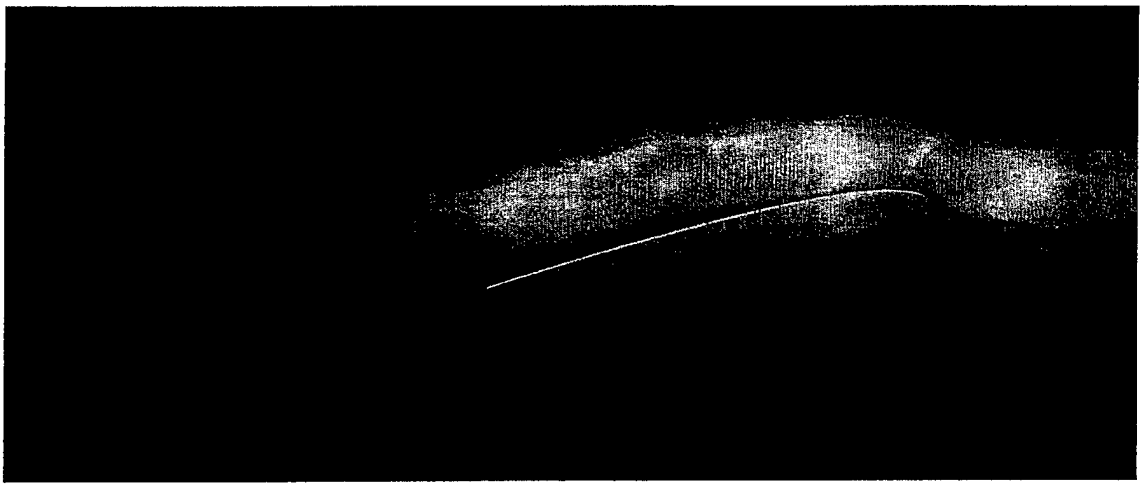

Steady case α=10 deg

Pitching case, incidence downstroke, α=10 deg

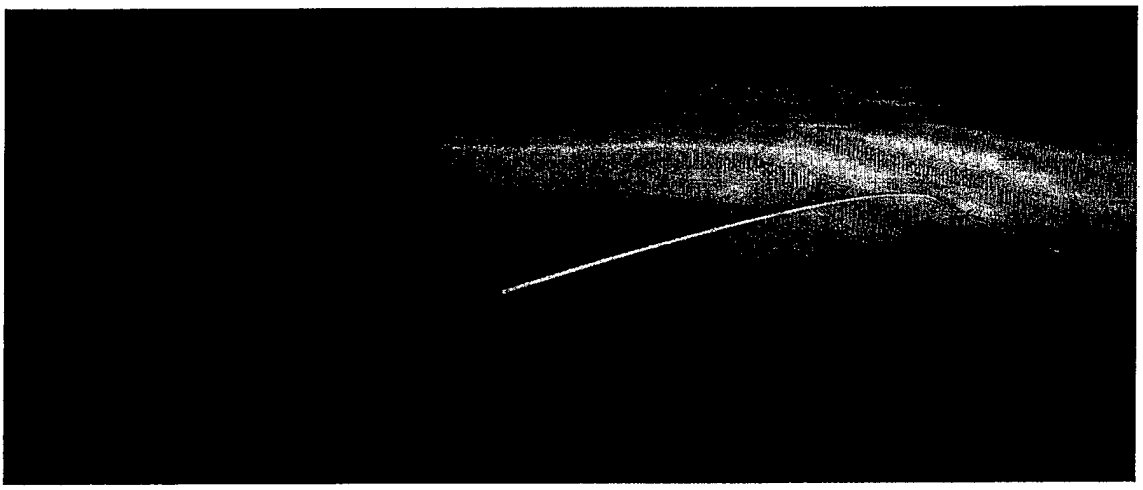

Pitching case, incidence upstroke, α=10 deg

Flow visualization around a NACA0012 airfoil, $R_e=10^5$

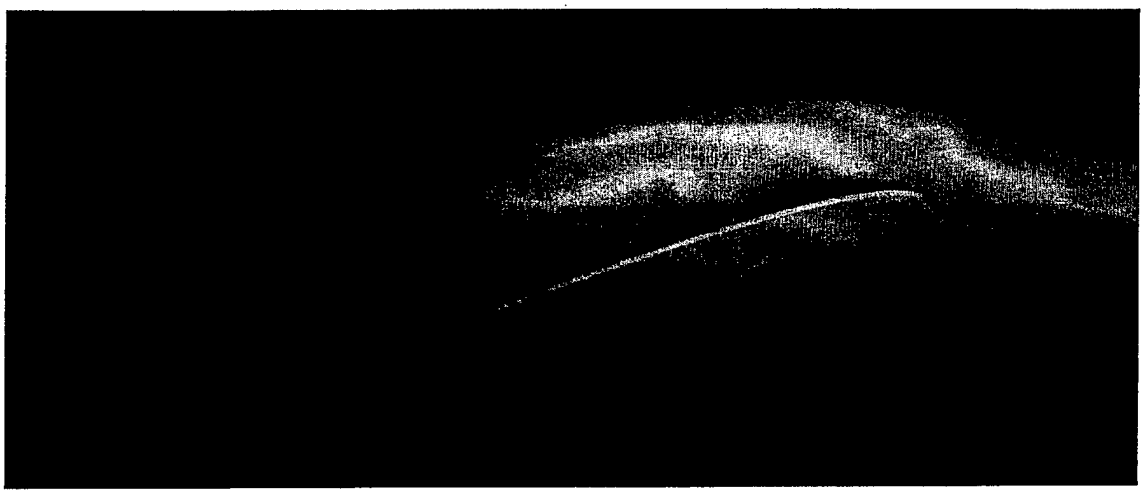

Steady case α=14 deg

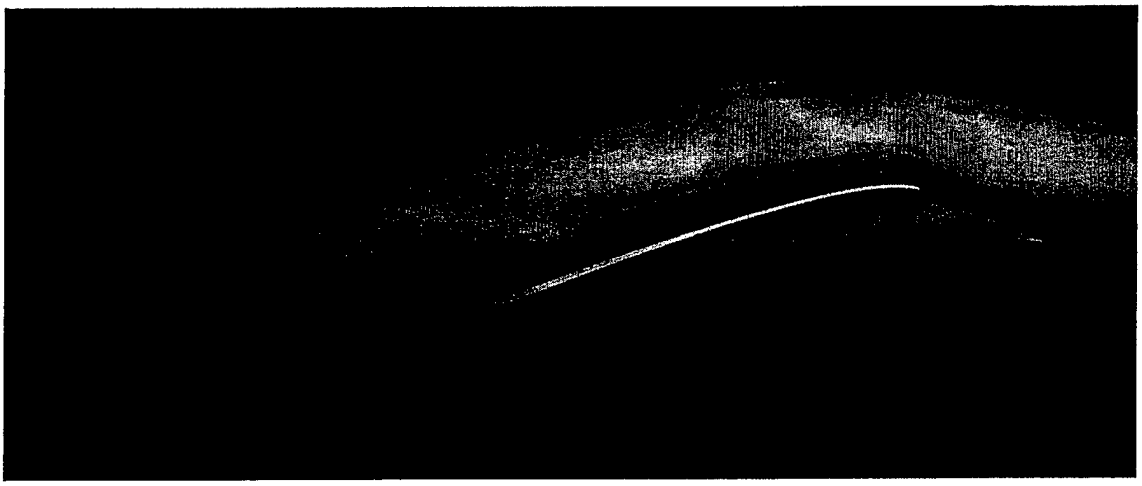

Pitching case, incidence downstroke, α=14 deg

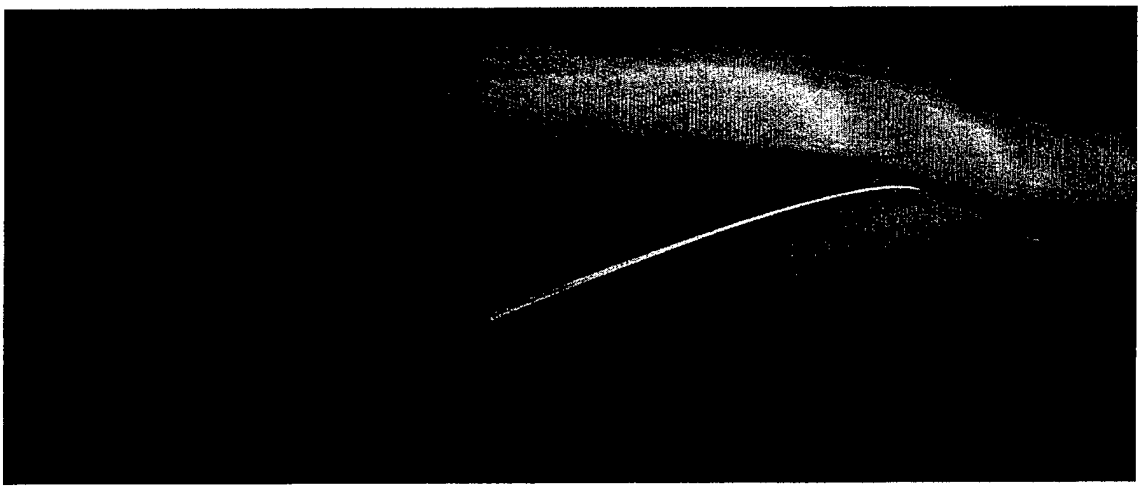

Pitching case, incidence upstroke, α=14 deg

Flow visualization around a NACA0012 airfoil, $R_e=10^5$

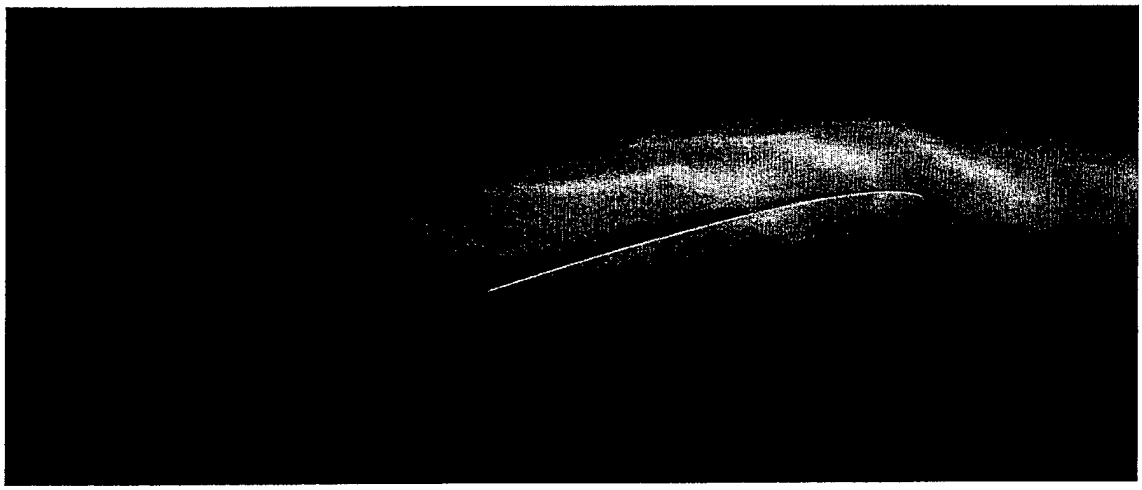

Steady case α=10 deg

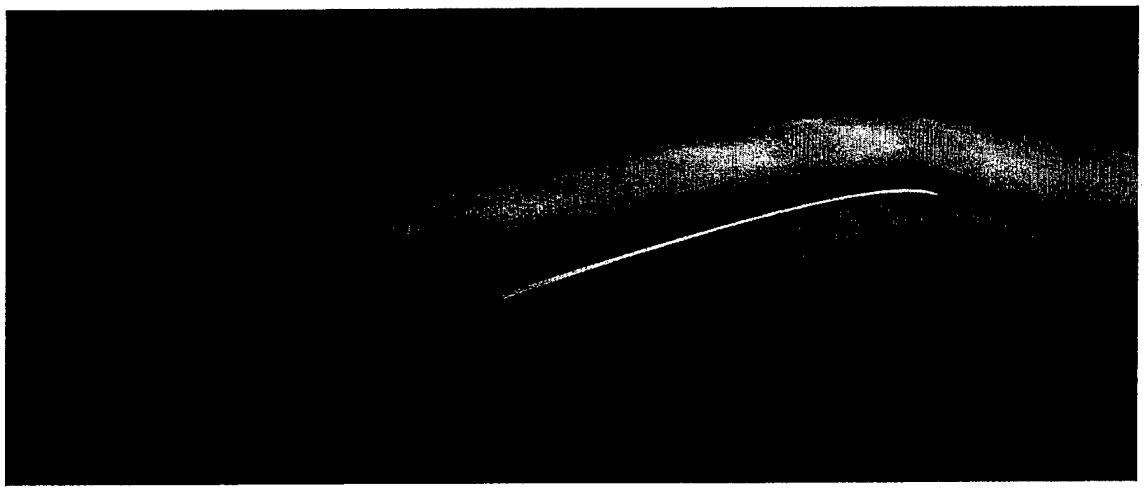

Pitching case, incidence downstroke , α=10 deg

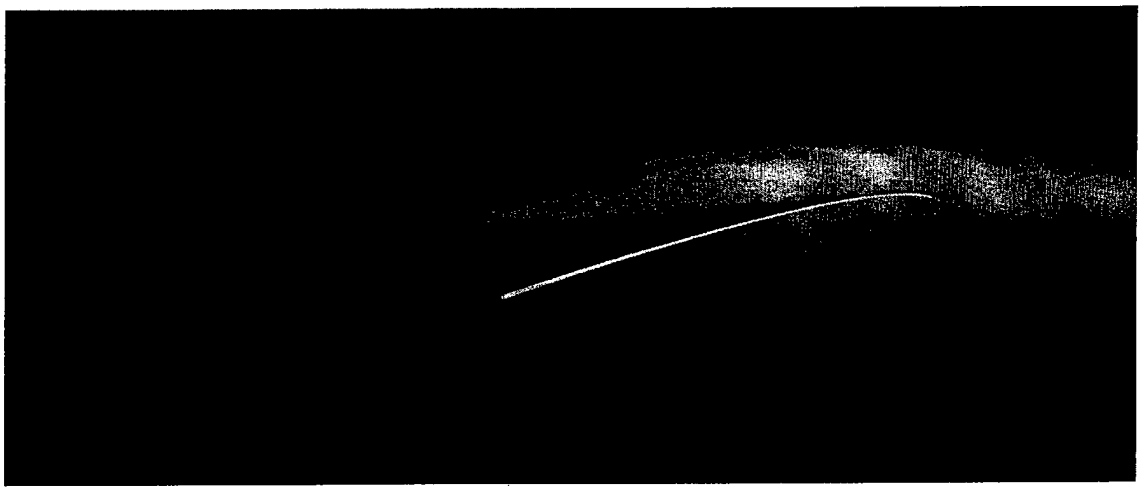

Pitching case, incidence upstroke , α=10 deg

Flow visualization around a NACA0012 airfoil, R_e=2 10^5

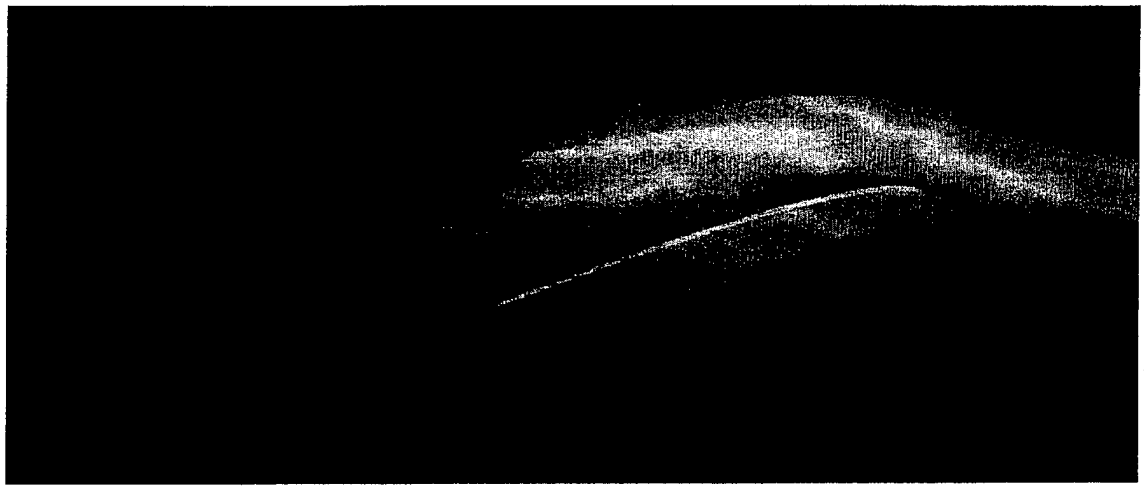

Steady case α=14 deg

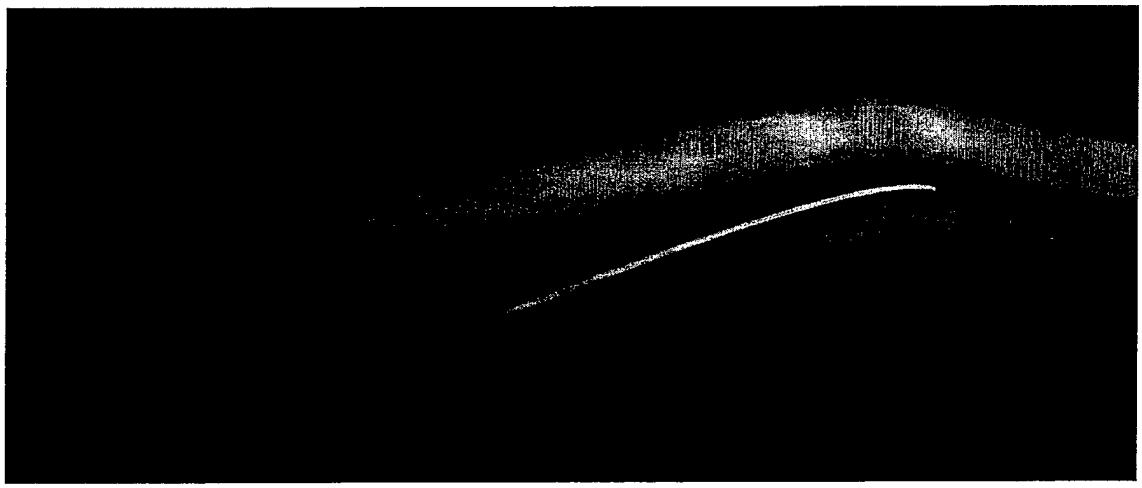

Pitching case, incidence downstroke, α=14 deg

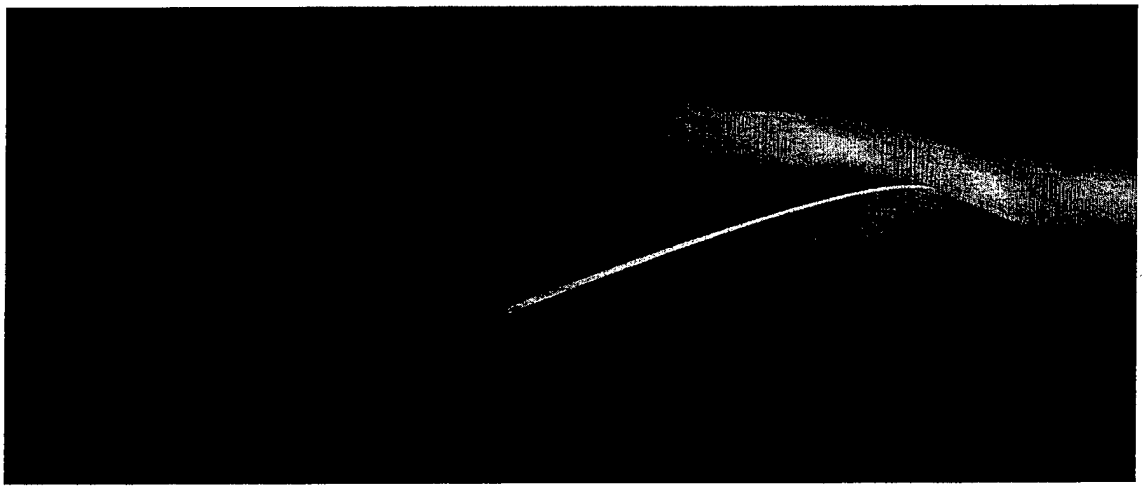

Pitching case, incidence upstroke, α=14 deg

Flow visualization around a NACA0012 airfoil, R_e=2 10^5

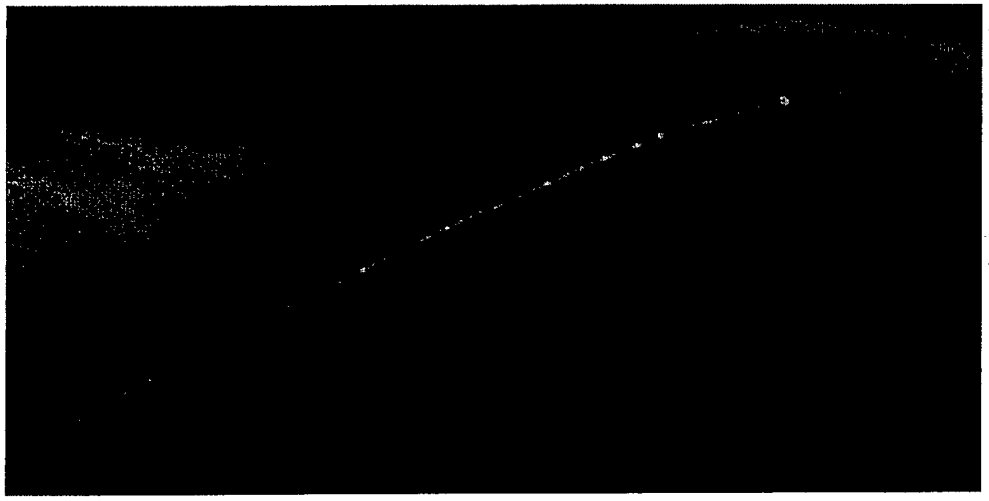

Steady case α=18 deg

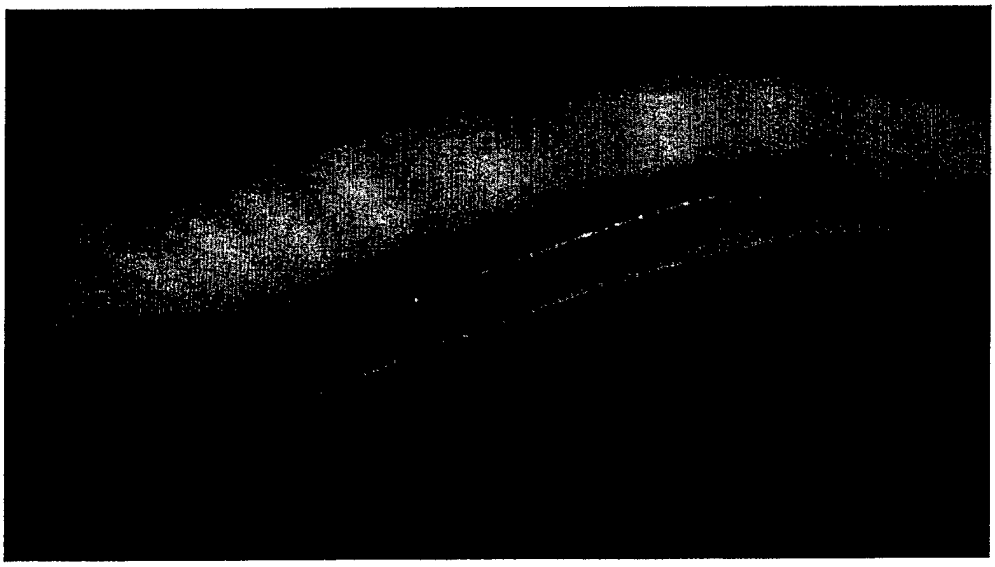

Pitching case, incidence downstroke, α=18 deg

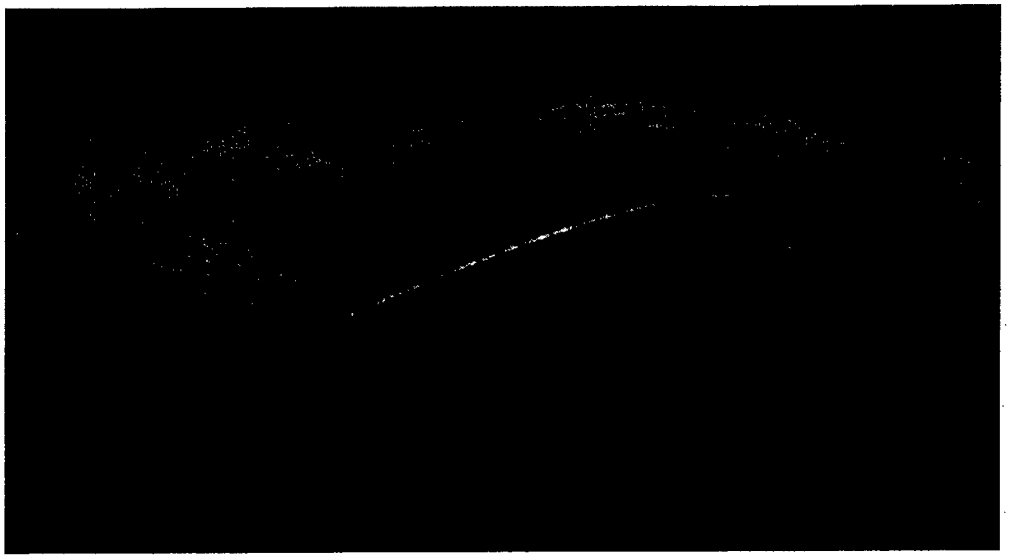

Pitching case, incidence upstroke , α=18deg

Flow visualization around a NACA0012 airfoil, Re= 10^6

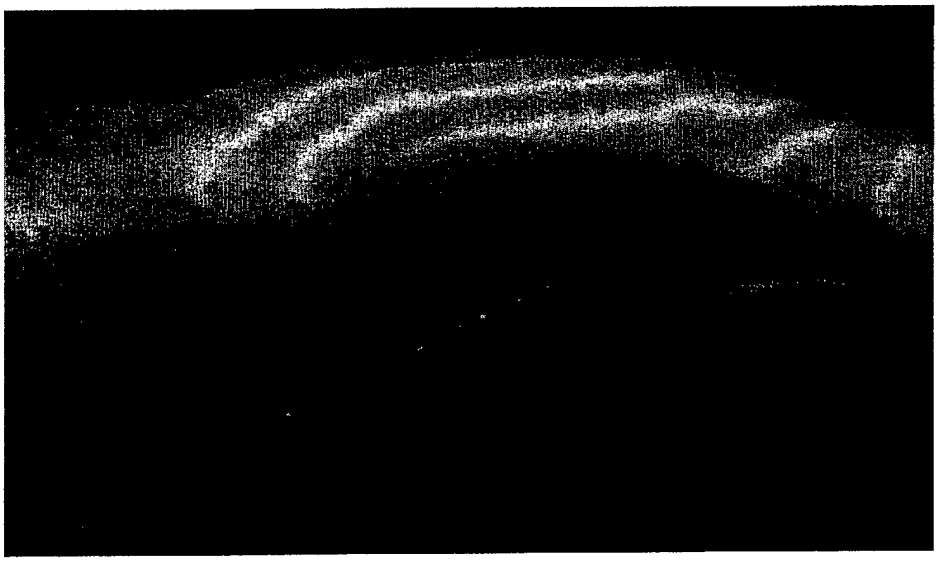

Steady case α=21 deg

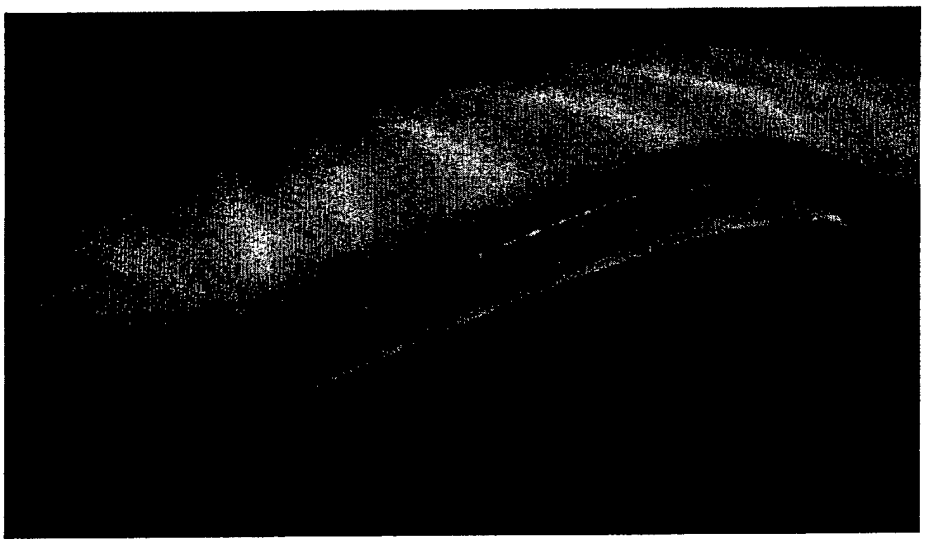

Pitching case, incidence downstroke, α=21 deg

Pitching case, incidence upstroke, α=21deg

Flow visualization around a NACA0012 airfoil, $Re=10^6$

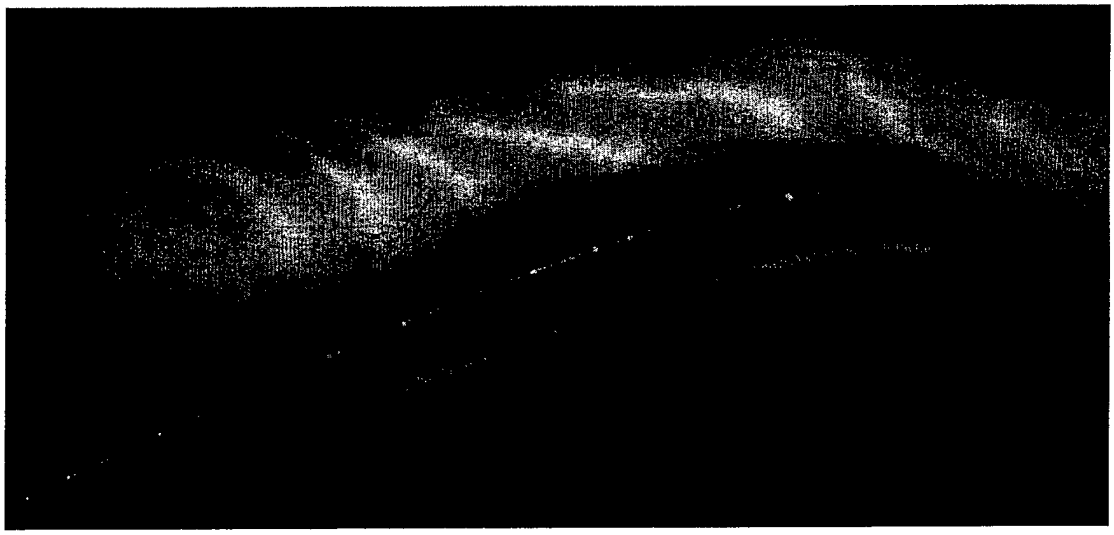

Steady case α=16 deg

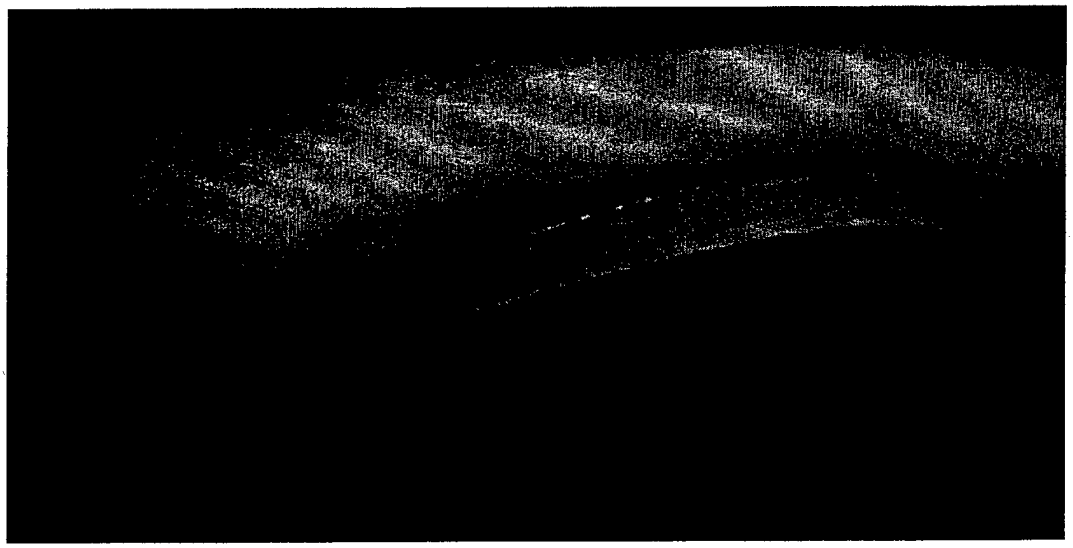

Pitching case, incidence downstoke, α=16deg

Flow visualization around a NACA0012 airfoil, Re= 10^6

Fig.11

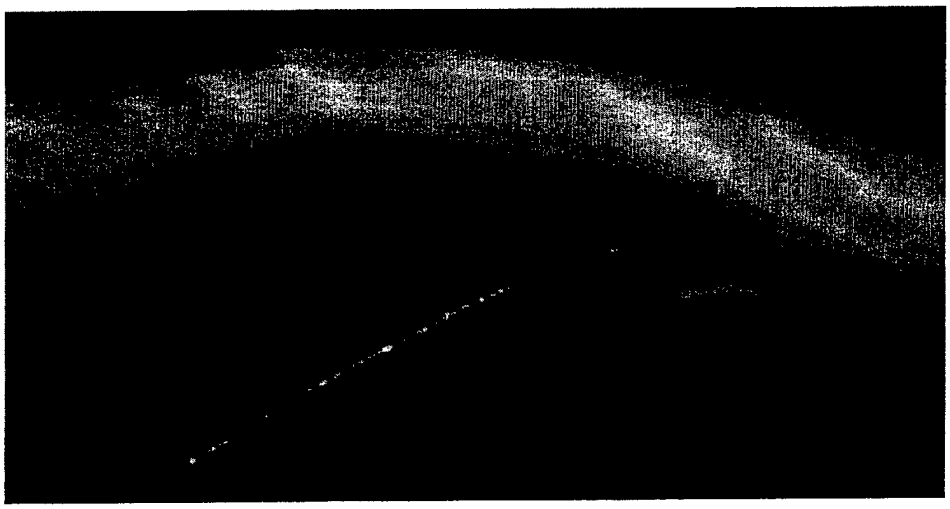

Steady case α=27 deg

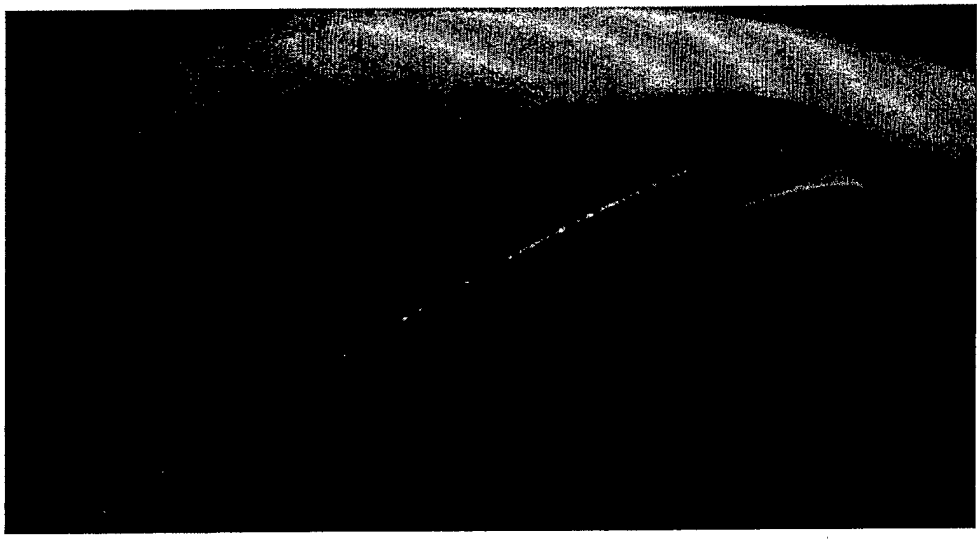

Pitching case, α=27 deg

Flow visualization around a NACA0012 airfoil, Re= 10^6

VELOCITY RECORDS: x/C=0.1

Fig.12

$\alpha=6\pm6$; $k=0.188$; $Re=10^5$

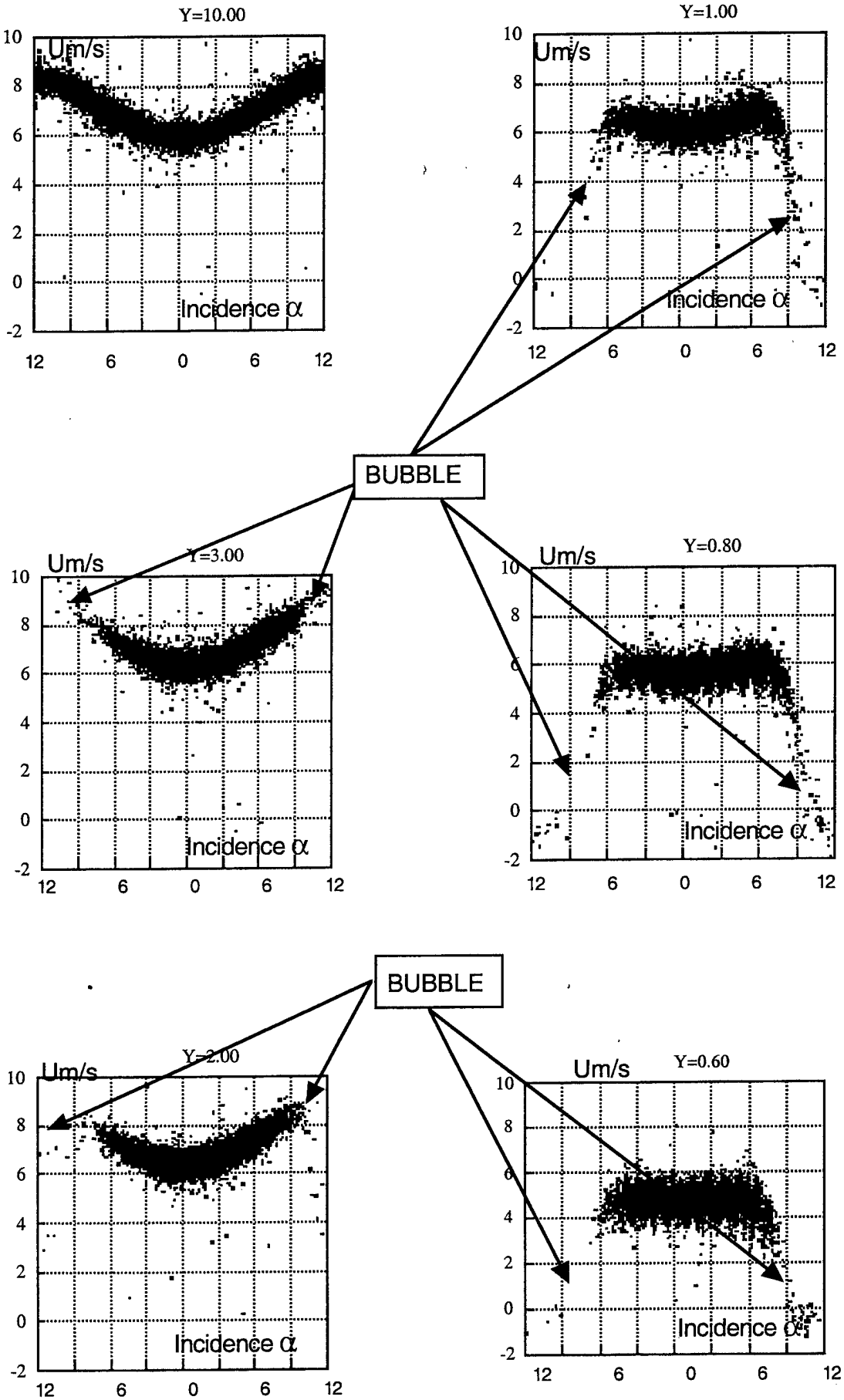

Fig. 13

Bubble dimension with incidence

α_0=6; $\Delta\alpha$=±6; Re=10^5; k=0.188

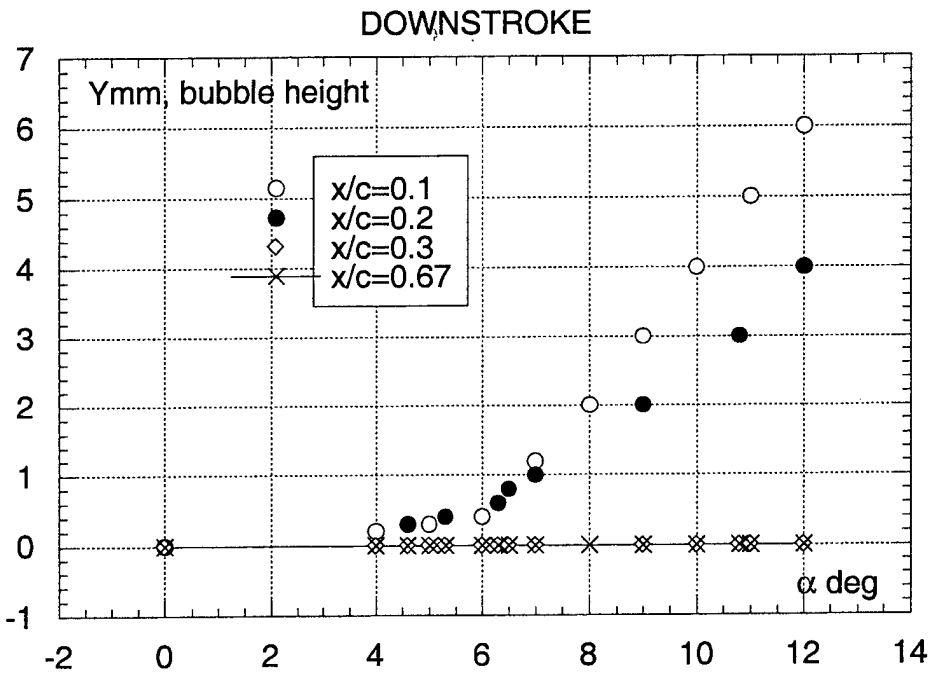

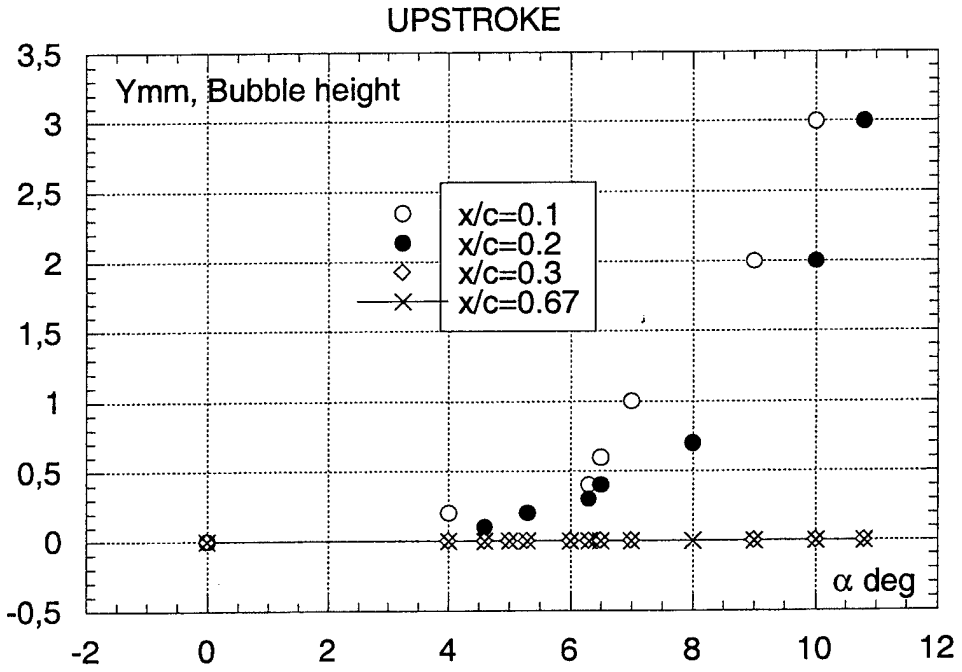

Longitudinal velocity U(Y, α)

α=6±6; Re=10^5; k=0.188

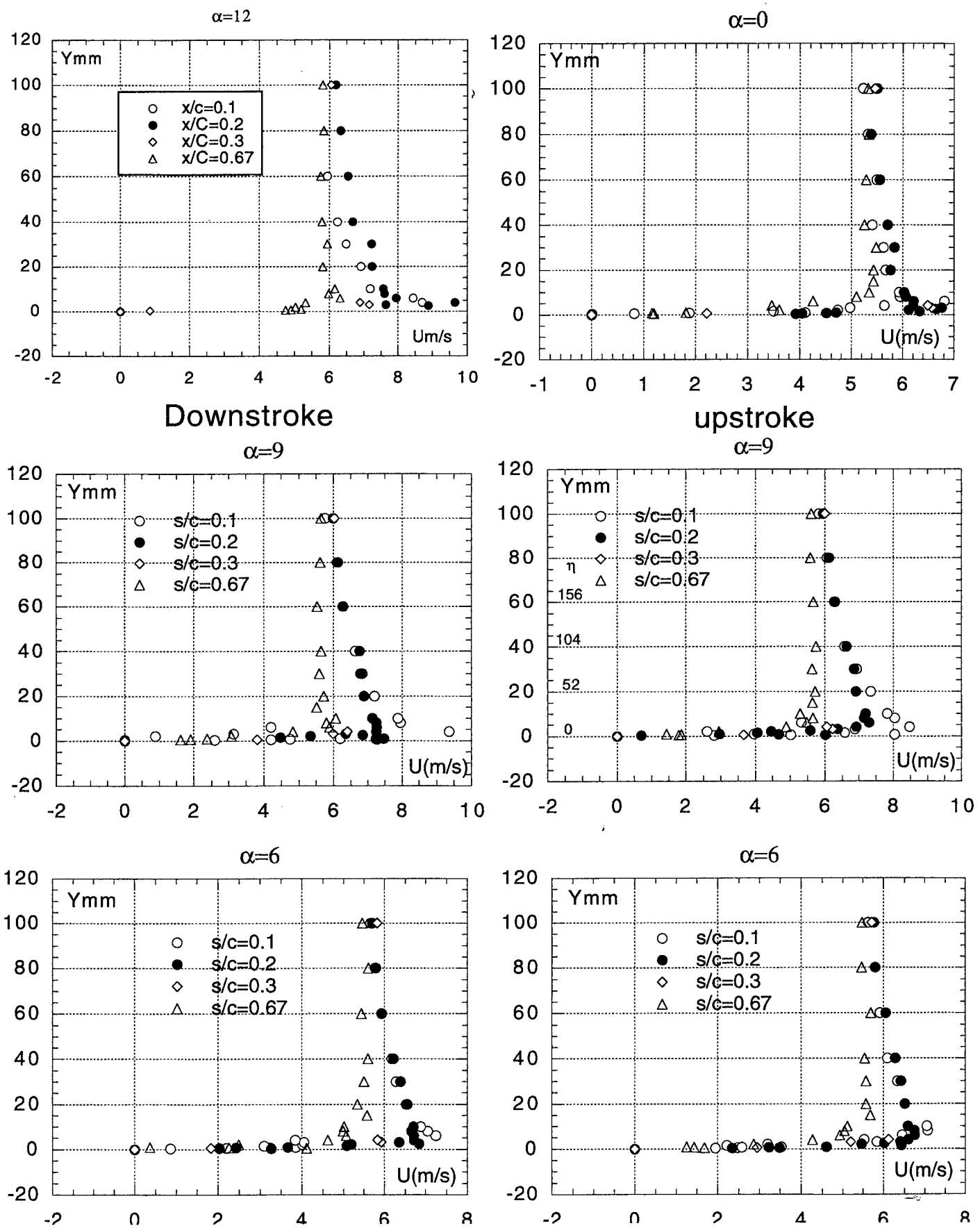

Fig.15

VELOCITY PROFILES IN THE BUBBLE

Pitching motion: α= 9deg downstroke

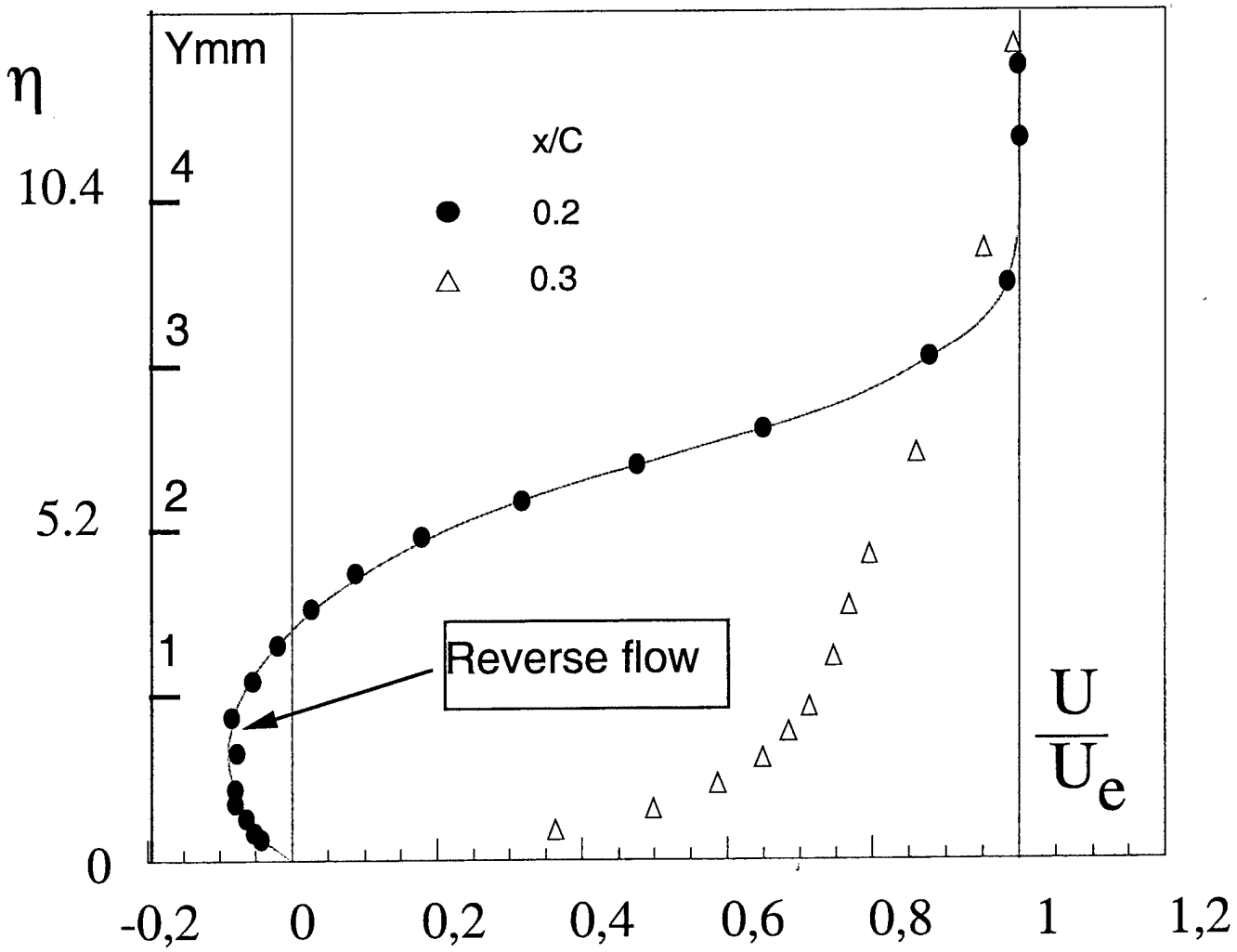

Fig.16

SEPARATION BUBBLE: VISUALIZATION AND THICKNESS DEDUCED FROM VELOCITY RECORDS

α_0= 16deg; $\Delta\alpha$= 6 deg; k=0.188; Re=10^5

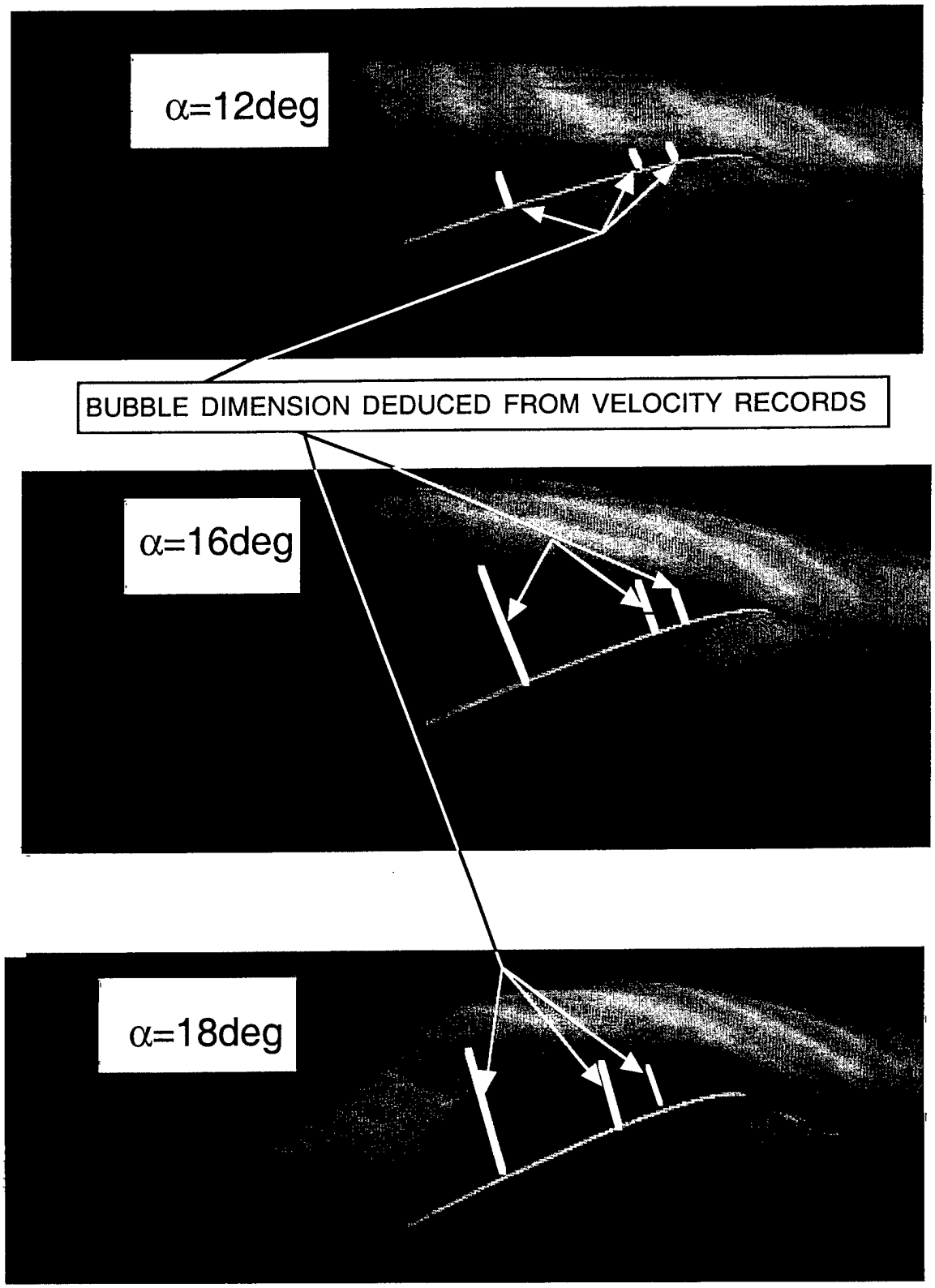

Longitudinal velocity U(Y, α)

α=15±6; Re=10^5; k=0.188

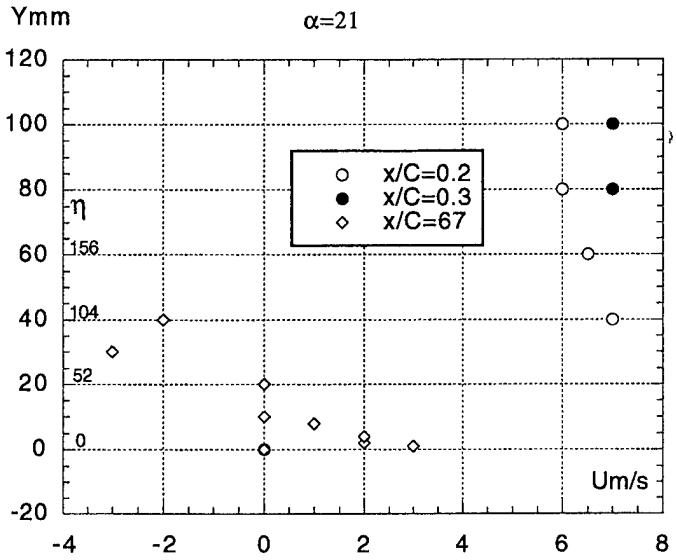

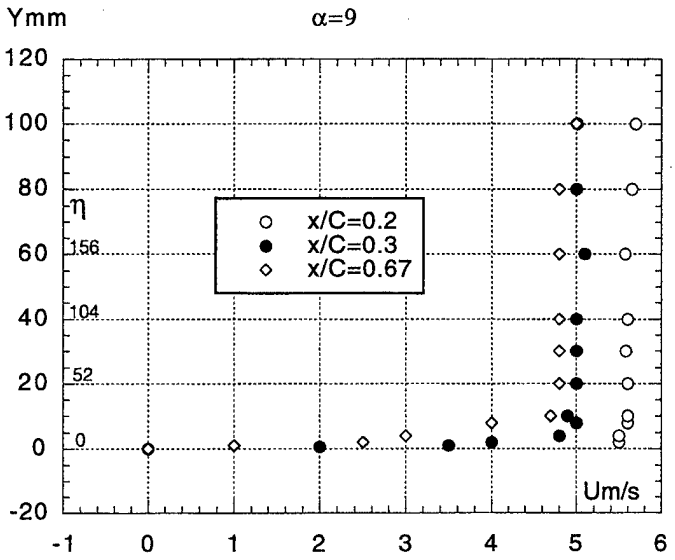

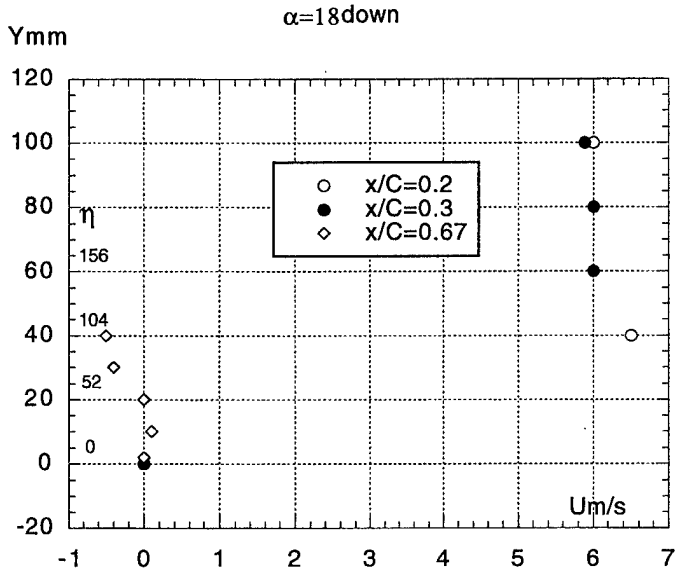

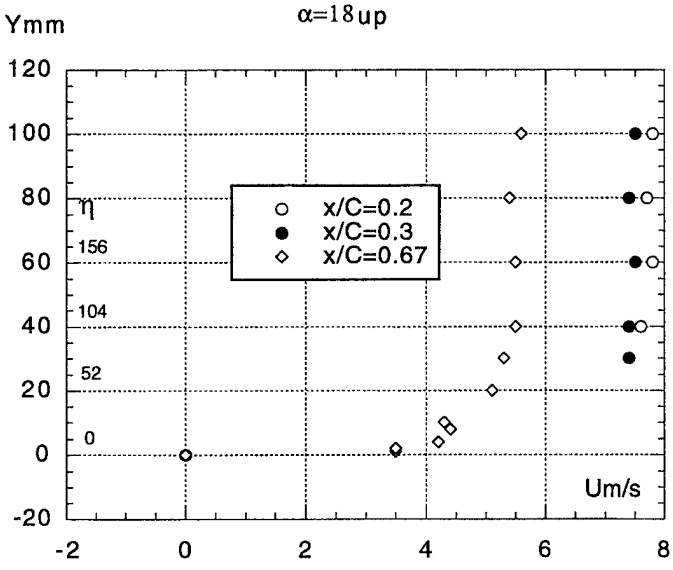

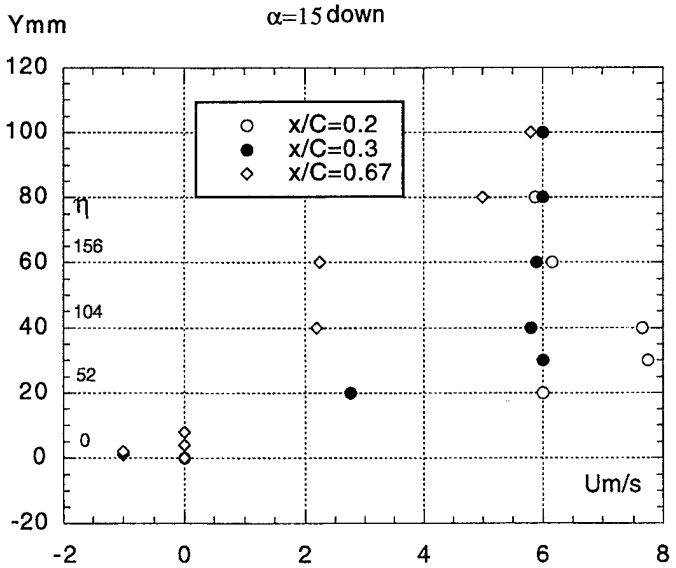

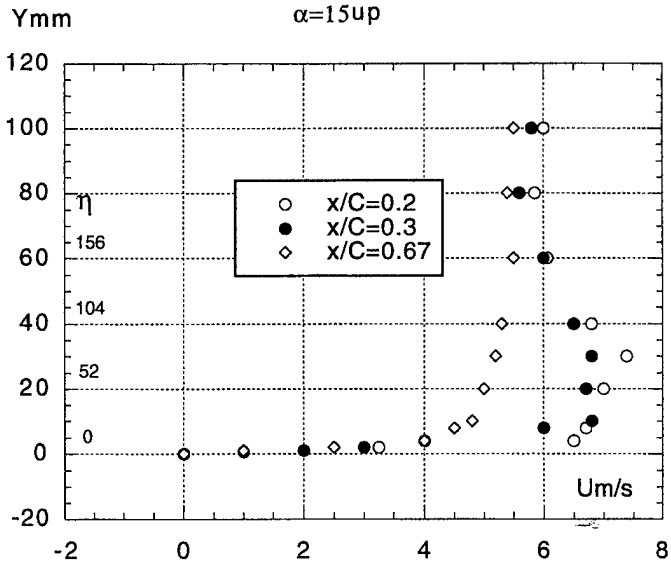

Velocity records

$\alpha=21\pm6$; $Re=10^6$; $k=0.18$

Y=80mm

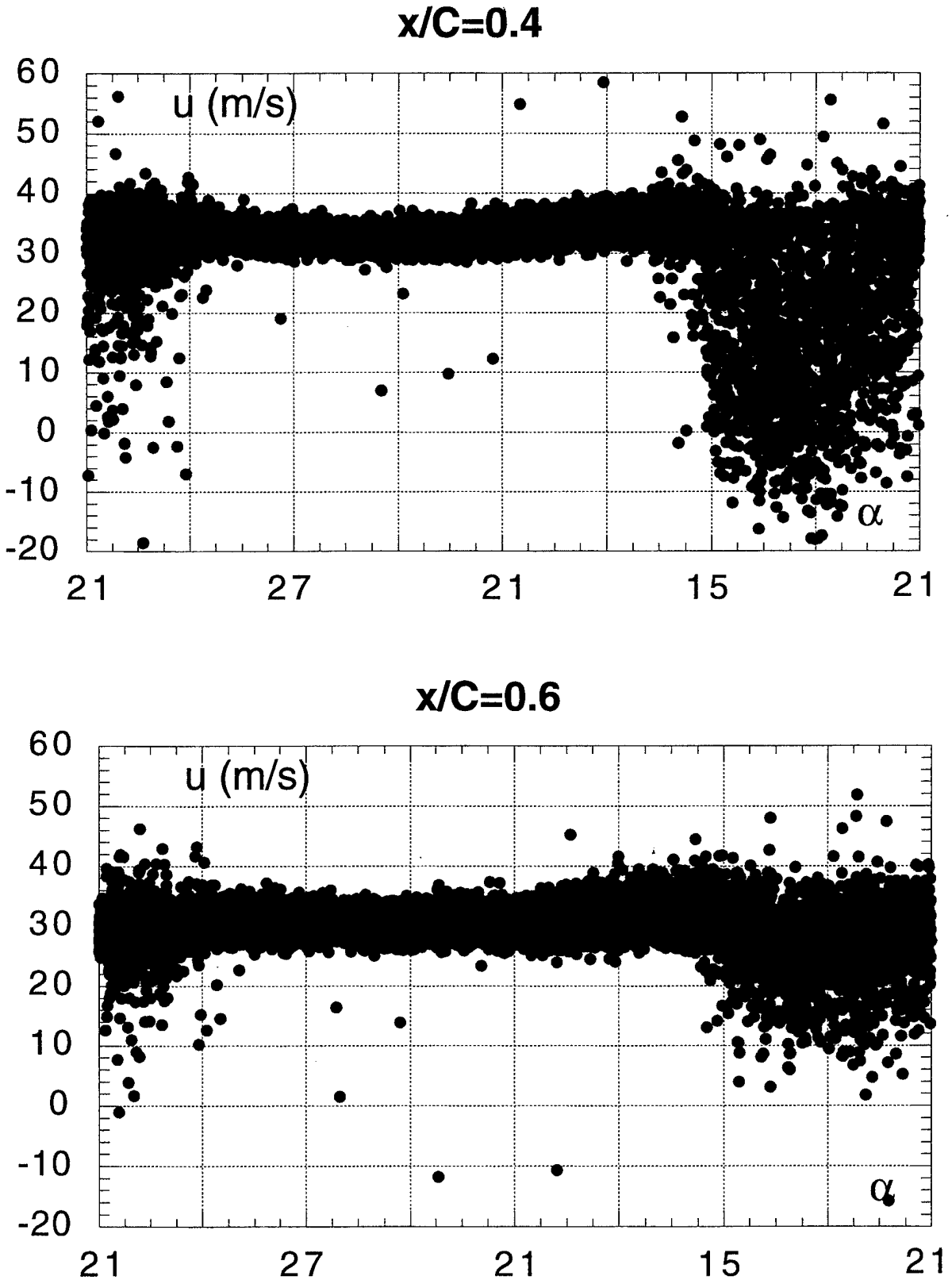

Longitudinal velocity U(Y, α)

α=21±6; Re=10^6; k=0.188

α=27

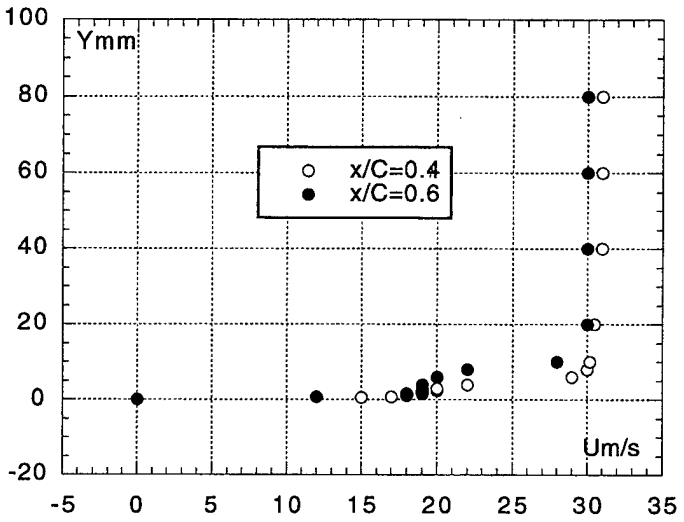

α=21down

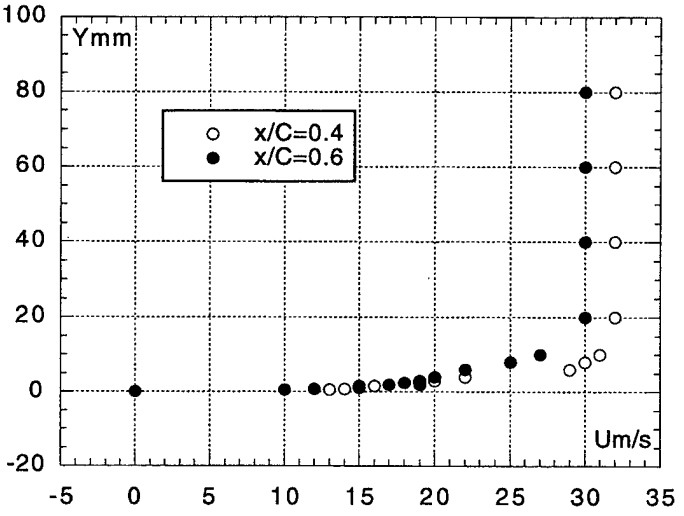

α=18down